Nanoparticles at fluid interfaces

2007 J. Phys.: Condens. Matter 19 413101

(http://iopscience.iop.org/0953-8984/19/41/413101)

IOP PUBLISHING JOURNAL OF PHYSICS: CONDENSED MATTER

J. Phys.: Condens. Matter **19** (2007) 413101 (33pp) doi:10.1088/0953-8984/19/41/413101

TOPICAL REVIEW

Nanoparticles at fluid interfaces

F Bresme[1] **and M Oettel**[2]

[1] Department of Chemistry, Imperial College London, SW7 2AZ, UK
[2] Institut für Physik, WA331, Johannes-Gutenberg-Universität Mainz, 55099 Mainz, Germany

E-mail: f.bresme@imperial.ac.uk and oettelm@uni-mainz.de

Received 19 June 2007
Published 10 September 2007
Online at stacks.iop.org/JPhysCM/19/413101

Abstract

Nanoparticles at fluid interfaces are becoming a central topic in colloid science studies. Unlike in the case of colloids in suspensions, the description of the forces determining the physical behavior of colloids at interfaces still represents an outstanding problem in the modern theory of colloidal interactions. These forces regulate the formation of complex two-dimensional structures, which can be exploited in a number of applications of technological interest; optical devices, catalysis, molecular electronics or emulsions stabilization. From a fundamental viewpoint and typical for colloidal systems, nanoparticles and microparticles at interfaces are ideal experimental and theoretical models for investigating questions of relevance in condensed matter physics, such as the phase behavior of two-dimensional fluids.

This review is a topical survey of the stability, self-assembly behavior and mutual interactions of nanoparticles at fluid interfaces. Thermodynamic models offer an intuitive approach to explaining the interfacial stability of nanoparticles in terms of a few material properties, such as the surface and line tensions. A critical discussion of the theoretical basis, accuracy, limitations, and recent predictions of the thermodynamic models is provided. We also review recent work concerned with nanoparticle self-assembly at fluid interfaces. Complex two-dimensional structures varying considerably with the particle nature have been observed in a number of experiments. We discuss the self-assembly behavior in terms of nanoparticle composition, focusing on sterically stabilized, charged and magnetic nanoparticles. The structure of the two-dimensional assemblies is a reflection of complex intercolloidal forces. Unlike the case for bulk colloidal suspensions, which often can be described reasonably well using DLVO (Derjaguin–Landau–Verwey–Overbeek) theory, the description of particles at interfaces requires the consideration of interfacial deformations as well as interfacial thermal fluctuations. We analyze the importance of both deformation and fluctuations, as well as the modification of electrostatic and van der Waals interactions. Finally, we discuss possible future directions in the field of nanoparticles at interfaces.

(Some figures in this article are in colour only in the electronic version)

Contents

1. Introduction

The last decade has witnessed an increasing interest in the investigation of colloidal nanoparticles adsorbed at fluid interfaces. A driving force for such studies is the range of applications of such particles. Due to their small dimensions their properties depart significantly from the properties of macroscopic materials. Hence, metallic and semiconducting nanoparticles have been targeted as building blocks for materials with specific mechanical, optical, and magnetic properties [1]. The self-assembly of nanoparticles at fluid interfaces (liquid–vapor and liquid–liquid) has enabled the preparation of high quality two-dimensional crystals. In particular Langmuir trough techniques provide a means to tune the interparticle distances and facilitate the transfer of the crystal monolayers to solid substrates [2]. Particles adsorbed at interfaces also play an important role in industrial processes concerned with foams and emulsion [3, 4]. It has been known for many years that the large stability of particles at interfaces can be exploited to tune the stability of emulsions. At the same time it is now well established that particles at interfaces can be used to study also some basic problems in condensed matter physics, such as the physical behavior of two-dimensional crystals [5–7].

The large stability of colloidal microparticles at the water–air interfaces was already discussed by Pieranski [5]. Considering the surface energies of the particle–air, particle–water and air–water interfaces Pieranski noted that the activation energy for particle detachment scales quadratically with the colloid radius, being of the order of 10^7 times the thermal energy for polystyrene microparticles adsorbed at the water–air interface. This high stability enables the formation of two-dimensional [5, 8], and pseudo-two-dimensional structures [9]. The strong repulsions between the colloids, necessary to prevent coagulation in the colloidal solutions, can be introduced through steric interactions or surface charges. Once the

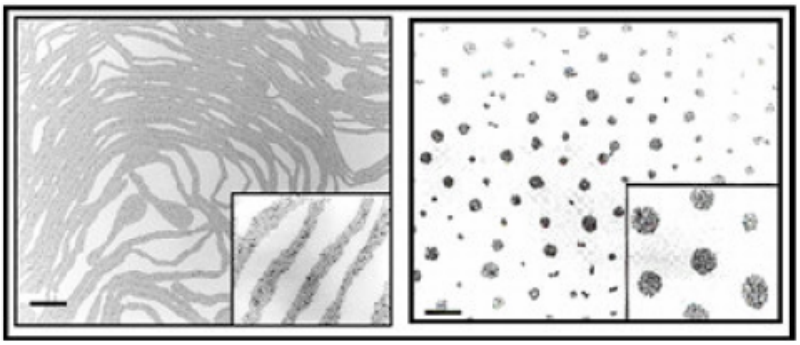

Figure 1. TEM micrographs showing the formation of clusters and stripelike arrays of alkylthiol passivated silver nanocrystals (4–6 nm diameter) [19]. Reprinted figure with permission from Sear *et al* [19]. Copyright 1999 by the American Physical Society.

colloids become complexly shaped and/or the intercolloidal potential is attractive for a certain range of colloid–colloid distances [10], the phenomenology of self-assembly patterns is greatly enriched. For colloidal objects with sizes >10 μm possible orientation dependent attractions are well understood in terms of flotation forces, for experimental realizations see [11, 12].

In comparison with colloidal 'microparticles', the stability of 'nanoparticles' at interfaces is greatly reduced, with activation energies of the order of 10–100 times the thermal energy. Nanoparticles are therefore more sensitive to thermal fluctuations than microparticles. Indeed the competition between thermal fluctuations and interfacial forces gives rise to particle size dependent self-assembly [13]. Also, the stability of nanoparticles at fluid interfaces exhibits a stronger dependence with interfacial forces such as the line tension, the free energy of the three-phase line introduced originally by Gibbs [14]. Recent investigations using thermodynamic models and computer simulations have illustrated the potential relevance of the line tension in describing the behavior of spherical and nonspherical nanoparticles [15–17]. For nonspherical particles it has been predicted that line tensions of the order of 10^{-11}–10^{-10} N can completely destabilize nanoparticles of elongated shape [17], illustrating the importance of particle shape as a variable determining surface activity at fluid interfaces.

Several experimental studies of nanoparticles at interfaces have reported the formation of unusual two-dimensional structures [18, 19], motivating new theoretical approaches to colloidal interactions beyond the traditional bulk considerations. It has been shown that silver passivated nanoparticles (quantum dots) at the air–water interface spontaneously form clusters and stripelike arrays [18] (cf figure 1). Some of these patterns are reminiscent of the structures formed by charged polystyrene microparticles at the air–water interface [20], although the interactions between nanoparticles and microparticles are expected to be rather different. It has been argued that the interplay between attractive van der Waals forces and a long range repulsive tail could be responsible for limiting the cluster size and induce the pattern formation [19]. The physical origin of these interactions is nonetheless a matter of debate, given the lack of experimental and theoretical work that can explain them unequivocally. Thus, a major challenge is the development of theories and robust microscopic models that provide an understanding of the interfacial interactions between nanoparticles and that clearly elucidate the differences between these interactions and the interactions of nanoparticles in bulk phases. As a matter of fact such differences are illustrated by the case of charged colloids. Screened Coulombic interactions will be modified due to the existence of dielectric

discontinuities (for instance air–water and oil–water interfaces). Similarly the net van der Waals interactions will depend on the properties of two solvent phases (not just one) which complicates the application of theoretical treatments to model these interactions at interfaces. In addition to the Coulombic and dispersion interactions considered in the context of bulk colloidal theories such as DLVO [21], new types of interactions connected to the interface deformation also arise. Hence, capillary forces are expected to play a role in the self-assembly of nanoparticles at interfaces. Such interfacial deformations are well understood in the case of macroscopic particles [22] where the interface deformation is induced by the particle weight. However, gravity plays a negligible role for nanometer size particles. Nevertheless at these small scales, immersion forces (arising for particles partially immersed in thin liquid films) may play a significant role [22]. Additionally electric field induced capillary interactions of charged particles at interfaces may emerge [23, 24]. These have been derived for the case of micrometer size particles; for high charge densities on colloid surfaces (around one elementary charge e per nm^2) they appear to be relevant also for the nanosized particles. Moreover, particle topology [25] and particle shape [10] can induce local interfacial deformations with strong anisotropic capillary forces between particles. In addition to the effect of static interface deformations, thermal fluctuations of the interface position are expected to add a nonnegligible contribution to the interactions between particles at interfaces [26, 27]. Finally, on very short separation between the colloids, the correlations between the fluid molecules will also induce general 'solvation' forces that may differ from the solvation or depletion forces observed in bulk colloidal suspensions due to the specific molecular correlations in the interface zone.

Closely related to the behavior of colloids at interfaces are the interactions of biological macromolecules, proteins and viruses, as well as nanoparticles adsorbed at membranes. Static capillary and fluctuation effects (equivalent to the case of fluid interfaces) in the mutual interactions between membrane enclosures exist; surveys on this topic can be found e.g. in [22, 28]. Recent experiments of proteins adsorbed at air–water interface indicate that the partial denaturation undergone by proteins may play a role in enhancing their stability at the interface [29]. On the other hand the interactions between nanoparticles and biological tissues are becoming the central topic of a new field of research, *nanotoxicology*. It is known that particles can adsorb at the lungs, and they can be responsible for a number of respiratory disorders. The retention of the particles at biological tissues depends on a number of variables; particle size, shape, surface properties, and the mechanical properties of the biological tissues. In a recent work it has been noted that very small particles, 6 μm and smaller, tend to be retained at the conducting airways for periods longer than one day [30].

From the introductory discussion above, it emerges that the investigation of nanoparticles at interfaces offers numerous challenges to theorists as well as experimentalists. For a start the *in situ* observation and characterization of nanoparticles at fluid interfaces is more difficult than that of micrometer particles, for which optical methods can be employed. Moreover, a detailed view of the interfacial structure around nanoparticles (and also microparticles) is difficult to obtain. Consequently, a full microscopic understanding of the interactions acting between nanoparticles at interfaces requires a dual approach with experiment and theory closely working together.

In this work we review the current status of research on nanoparticles at interfaces. We consider both experimental and theoretical studies focusing on nanoparticle sizes in the range $1 \ldots 10^3$ nm. The investigations of the larger nanoparticle sizes ($\approx$1 μm) are useful to rationalize the physical behavior observed for smaller particles, and also to illustrate the size dependent behavior observed in nanometer dimensions.

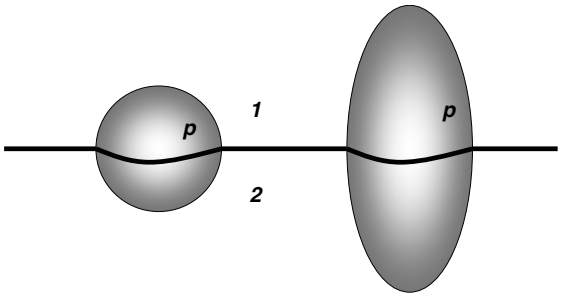

Figure 2. Sketch of nanoparticles 'p' adsorbed at a fluid interface. '1' and '2' refer to the two fluid phases.

2. Thermodynamic models of nanoparticles at interfaces

2.1. The free energy

Thermodynamic models, utilizing the standard thermodynamic bulk quantities and a few material parameters (surface and line tension, Tolman length...) provide a powerful and simple theoretical background to understand the adsorption behavior of particles at interfaces. Since these model abstract from the molecular nature of the solvent, their use seems more justified at the micrometer level where indeed adsorption phenomena can be discussed almost exclusively through surface tension effects. Nonetheless, recent investigation using e.g. computer simulations [16, 31, 32] have indicated that the behavior of truly nanoscale particles can be described within a wide range of conditions by such a phenomenological thermodynamic model upon introduction of particle size dependent surface tensions and three-phase line tensions. However, the introduction of line tensions poses some conceptual problems which are not fully resolved yet (see below).

The free energy of a system consisting of a nanoparticle adsorbed at a fluid–fluid interface can be written as,

$$F = F(T, V, N_1, \ldots, N_m, X_1, \ldots, X_k) \tag{1}$$

where V is the volume of the system, N_i is the number of particles of species i ($i = 1, m$) and X_j represent additional extensive variables that characterize the system. For a nanoparticle adsorbed at a planar interface that separates two thermodynamic phases, 1 and 2 (see figure 2), the free energy is given by:

$$F = F(T, V, N_1, N_2, A_{12}, A_{\mathrm{p}1}, A_{\mathrm{p}2}, L) \tag{2}$$

where $A_{\mathrm{p}j}$ are the areas of the particle–fluid interface and A_{12} is the area of the fluid–fluid interface (e.g. liquid–liquid). L represents the three-phase line where the three phases meet [33].

The surface tension, $\gamma_{\mathrm{p}i}$ (associated to the interface between nanoparticle and fluid i), and the line tension, τ (associated to the nanoparticle–fluid–fluid contact line), are given by:

$$\gamma_{\mathrm{p}i} = \left(\frac{\partial F}{\partial A_{\mathrm{p}i}}\right)_{T,V,N_1,N_2,A_{12},A_{\mathrm{p}j\neq i},L} \tag{3}$$

$$\tau = \left(\frac{\partial F}{\partial L}\right)_{T,V,N_1,N_2,A_{12},A_{\mathrm{p}1},A_{\mathrm{p}2}}. \tag{4}$$

The free energy of the nanoparticle at the interface, F_{int}, is normally expressed with reference to the free energy of the particle immersed in one of the fluid phases, F_0:

$$F_{\mathrm{int}} = F(T, V, N_1, N_2, A_{12}, A_{\mathrm{p}1}, A_{\mathrm{p}2}, L) - F_0(T, V, N_1, N_2, A_{12}, A_{\mathrm{p}}) \tag{5}$$

where A_p is the total area of the particle. The explicit expression for the free energy in terms of the interfacial areas is,

$$F_{int} = (\gamma_{12}A_{12} + \gamma_{p1}A_{p1} + \gamma_{p2}A_{p2} + \tau L - A_{st}\gamma_{12}) - \gamma_{12}A_{12} - \gamma_{p1}A_p \tag{6}$$

where A_{st} is the interface area removed by the nanoparticle. Considering that the total area of the particle, A_p is constant $A_p = A_{p1} + A_{p2}$ equation (6) simplifies to:

$$F_{int} = (\gamma_{p2} - \gamma_{p1})A_{p2} - \gamma_{12}A_{st} + \tau L. \tag{7}$$

Equation (7) is very general and it can be used to investigate nanoparticles of different shapes. The equations for spherical particles were derived by Aveyard and Clint [15] who arrived at a compact expression of the free energy in terms of the immersion of the particle in one of the phases,

$$\overline{F} = -\tfrac{1}{4}(1 - \overline{h}^2) + \tfrac{1}{2}\cos\theta_0(1 - \overline{h}) + \tfrac{1}{2}\overline{\tau}\sqrt{1 - \overline{h}^2} \tag{8}$$

where $\overline{F} = F/(\gamma_{12}A_p)$, $A_p = 4\pi R^2$ is the area of a particle of radius R. The immersion $\overline{h} = h/R$ in equation (8) is defined such that $h = 0$ corresponds to the configuration where the center of mass of the particle is at the interface, i.e., when the contact angle defined by $\cos\theta_0 = (\gamma_{p2} - \gamma_{p1})/\gamma_{12}$ is 90°. The reduced line tension, $\overline{\tau}$ is given by:

$$\overline{\tau} = \frac{\tau}{\gamma_{12}\sqrt{A_p/4\pi}}. \tag{9}$$

More recently Faraudo and Bresme have extended the free energy expressions to the case of nonspherical particles [17]. This problem is more complicated than that of the spherical particle. Besides immersion depth, the particle orientation is an additional degree of freedom and for arbitrary particle orientation the fluid interface would not remain flat after minimizing the free energy. To avoid this complication, a generic model consisting of prolate and oblate particle was considered. The free energy of a prolate-shaped particle with one major axis (of length z_m) perpendicular to the interface and the other two main axes (of equal length r_m) in the interface plane (see figure 2) becomes,

$$\frac{F}{\gamma_{12}A_p} = -\frac{1}{4G}(1 - \overline{h}^2) + \cos\theta_0 A_{p2}(\overline{h}) + \overline{\tau}\frac{1}{2\sqrt{G}}\sqrt{1 - \overline{h}^2} \tag{10}$$

with the reduced immersion depth given by $\overline{h} = h/z_m$ and the surface area, $A_p = 4\pi r_m^2 G(\alpha = z_m/r_m)$, is defined in terms of an aspect ratio dependent function $G(\alpha)$:

$$G(\alpha) = \frac{1}{2} + \frac{\alpha^2}{4\sqrt{1-\alpha^2}}\ln\left(\frac{1+\sqrt{1-\alpha^2}}{1-\sqrt{1-\alpha^2}}\right) \qquad \text{if } \alpha \leqslant 1 \tag{11}$$

$$G(\alpha) = \frac{1}{2} + \frac{\alpha}{2\sqrt{1-\alpha^{-2}}}\arcsin(\sqrt{1-\alpha^{-2}}) \qquad \text{if } \alpha > 1. \tag{12}$$

It is easy to see that equation (10) reduces to equation (8) when $\alpha = 1$. Similar equations can be derived for other configuration, for which the main axes of the nanoparticle are located in the interface plane (see [17]). It is important to note that in the general case of nonspherical particles certain orientations result in an undulated contact line around the nanoparticles. This effect has been neglected in the thermodynamic treatments considered to date which assume a flat three-phase line. Nonetheless, a recent theoretical/simulation study has shown that this approximation is accurate in describing the adsorption behavior of nonspherical nanoparticles at liquid–liquid interfaces [34, 35].

After a discussion of some aspects of the theory and experimental determination of line tensions, we turn in section 3 to the application of the thermodynamic model introduced above to a range of situations concerned with spherical and nonspherical particles.

2.2. *Line tension of nanoparticles at fluid interfaces*

The line tension was introduced by Gibbs [14, 33] to define the excess free energy associated to the line where three phases meet. The accurate experimental measurement of the line tension has been a considerable challenge. In fact, the uncertainty in the order of magnitude of the line tension has generated a very large number of studies. The literature is very extensive, the interested reader is referred to a recent review devoted to the current status of the three-phase line tension [36]. Line tensions inferred from experiments span several orders of magnitude, 10^{-12}–10^{-6} N [36, 37], reflecting the variety of experimental techniques (which are all indirect) and the variety of materials used.

On theoretical grounds the line tension can be either positive or negative and it is expected to be a small force [33], 10^{-11} N. For simple fluids away from criticality, dimensional analysis gives $\tau \sim k_B T/\sigma$ where $\sigma \sim 0.1$ nm is a typical atomic length scale. See e.g. reference [38] for the calculation of the line tension of a liquid wedge using a microscopic density functional theory. It is not clear from the outset that the concept of line tension is unique, i.e. independent from notional shifts of the interfaces (which also shift the location of the contact line) that should be permitted within the molecularly diffuse interface region. Indeed, following reference [39], it is seen that the line tension introduced in the free energy model for a nanoparticle at the interface, equation (6), is affected by a notional change of the colloid–fluid interface, whereas line tensions inferred from measurements on droplets on substrates are unique to leading order (in the size of the droplet). Nevertheless, a relation between these two line tensions can be established [39].

The thermodynamic model introduced in the previous section indicates that small line tensions can be responsible for noticeable changes in the contact angle of nanoparticles at interfaces. This can be summarized in the so called 'modified' Young–Dupré equation, which can be obtained by minimization of the interfacial free energy with respect to the particle contact angle,

$$\cos\theta = \cos\theta_0 - \frac{\tau}{r\gamma_{12}} \tag{13}$$

$$\cos\theta = \cos\theta_0 \left[1 - \frac{\tau}{R\gamma_{12}\sin\theta}\right]^{-1}. \tag{14}$$

The first expression holds for a sessile drop on a solid surface, where r is the radius of the three-phase contact line. The second expression applies to spherical particles of radius R at a fluid interface. In both expressions $\cos\theta_0$ is the wetting coefficient given by Young's equation, $\cos\theta_0 = (\gamma_{p1} - \gamma_{p2})/\gamma_{12}$, where p refers to the nanoparticle or to a substrate. Although often used in the literature, these equations are somewhat phenomenological and should be regarded with caution as they suffer from the above mentioned dependence on notional shifts of the interfaces. For an invariant expression in the case of the droplet, see [39]. Nevertheless, equations (13) and (14) offer a simple way to estimate the effect of the line tension on the contact angle. The line tension effect becomes irrelevant for large enough particles or droplets, but can otherwise be significant for nanoparticles ($R \sim \tau/\gamma_{12}$). In fact, lowering the size of nanoparticles may induce their detachment from fluid interfaces provided the line tension is large enough [40, 15–17]. For the case of droplets on surfaces, several experiments have addresses the effect of the line tension on their wetting behavior, yielding this enormous spread of line tension values between 10^{-12}–10^{-6} N [37, 36]. Wang *et al* [45] have investigated liquid droplets of size $\sim$1 μm. The analysis of the experimental data yields a line tension of the order of 10^{-10} N (positive or negative), changing sign when the wetting transition is approached. This behavior agrees with several theoretical predictions [41, 42]. A similar physical behavior has been observed in experiments of 'micron' hexaethylene glycol droplets on silicon, where line

tensions of the order of 10^{-10} N [43] have been reported. Recent experiments [44] using micron and nanosized alkane droplets at silanized silicon surfaces have questioned the validity of equation (13). The line tension was estimated in these experiments using the method discussed in [38]. The line tensions were *negative* and of the order of 10^{-12} N.

With regard to particles at interfaces, estimates of the line tension of micron size spherical glass beads at liquid–vapor interface suggest that the line tensions should not be larger than 10^{-8} N [46]. The results of experiments on spherical particles adsorbed at the air–water interface have been reviewed in [37], quoting line tensions in the range 10^{-12}–10^{-9} N. As an example, line tensions of the order of 10^{-11}–10^{-10} N [47] have been measured for micrometer size glass spheres at the air–water interface, and a considerable spread of 10^{-12}–10^{-9} N has been reported [48, 37] for the case of palladium particles. Exceptionally large values have been reported by Yakubov *et al* [49], of the order of 10^{-8} N for silica coated particles and -10^{-6} N for polystyrene particles. These experiments were performed using an atomic force microscope unlike the previous results which are mostly based either on particle attachment/detachment. Most of these experiments are based on microparticles and among them many of the techniques rely on optical microscopes to deduce the contact angle from geometric measurement. There are obvious limitations to extend these methods to the nanoparticle domain. Moreover, systematic effects (independent from line tensions) which lead to a possible change of the observed contact angle with respect to Young's angle have rarely been taken into account. Such effects may be caused by the presence of surfactant, roughness of particles and electric fields originating from surface charges.

As a consequence it is fair to say that there are no truly reliable measurements of the line tension of nanoparticles at interfaces. A notable exception with some perspective for nanoparticle line tension is the work by Aveyard and co-workers [50]. These authors developed a technique that is based on surface pressure measurements. This technique has been used to estimate the contact angle and size of stabilized calcium carbonate nanoparticles ($\approx$3 nm diameter). In this instance the line tension was also estimated to be of the order of 10^{-11} N. The interpretation of the experiments relies on the idea that the particles are expelled from the interface at the collapse pressure—occurring for dense packing, which is geometrically determined by the contact angle. However, it has been shown that this assumption is not always correct. Computer simulations [51, 52] and also experiments [53] have shown that particle arrays do actually fold as an alternative mechanism to particle ejection.

As we attempted to show, the application of the corrected Young's equation to extract line tension values encloses some difficulties since measuring contact angles of sub micron particles is still nowadays a major challenge. As an alternative, nanoparticle contact angles have been computed using molecular dynamics simulations, of spherical structureless nanoparticles [16, 31, 32] as well as realistic (quantum dots) nanoparticles [54]. For the spherical particles, the line tension has been calculated using a free energy perturbation approach. The line tensions obtained from the simulations are in the range 10^{-12}–10^{-11} N and apply to particles with diameters ranging from 1 to 5 nm, adsorbed at liquid–vapor and liquid–liquid interfaces. The line tensions were both positive and negative, depending on the particle size and the interfacial tension of the fluid interfaces. In addition to quantifying the nanoparticle line tension, these molecular dynamics simulations provided a molecular view of the three-phase line (see figure 3) and enabled testing the validity of macroscopic approaches such as the Young's and modified Young's equation for the specific case of structureless nanoparticles at liquid–vapor and liquid–liquid interfaces. One conclusion from these studies was that Young's equation is surprisingly accurate in predicting the contact angle of small nanoparticles down to sizes of the order of 1–3 nm (as reflected in the smallness of the line tension values). The introduction of the line tension through the modified Young's equation further improved the

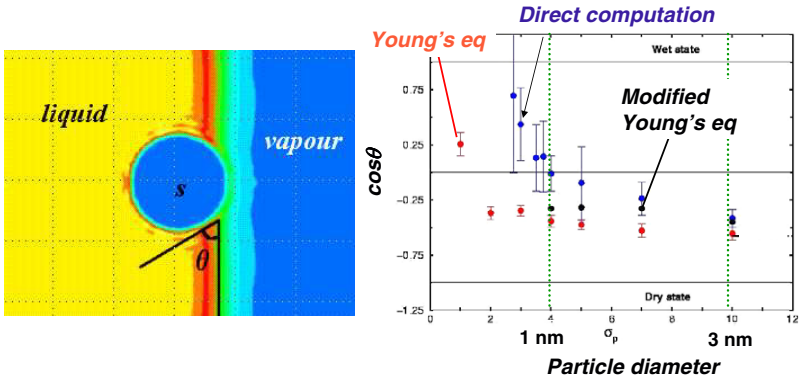

Figure 3. Left: Liquid–vapor density profile of a Lennard-Jones model ($\gamma_{lv} = 3$ mN m^{-1}) around a nanometer size particle of 3 nm diameter. The contact angle of the nanoparticle at the interface is indicated in the figure. Right: Variation of the contact angle with the nanoparticle diameter. Contact angles obtained directly from the simulation are compared with estimates from Young's and modified Young's equations. The contact angles converge for large nanoparticle sizes to the contact angle of the liquid with a planar wall, which corresponds to the limit of particle of infinite radius [16].

description of the contact angles but it was found that for very small particles the macroscopic approach breaks down.

3. Stability of nanoparticles at interfaces

3.1. Spherical particles

The thermodynamic model outlined in section 2 is completely general and can be applied to many problems concerned with particles at interfaces and also droplets on substrates. Widom [40] used a similar model to investigate the effect of the line tension on the contact angle between a micrometer size sessile drop and a solid substrate (see equation (13)). It was shown that large enough, positive values of the line tension, 10^{-10} N, can result in a discontinuous jump in the contact angle, inducing surface drying and therefore inhibiting droplet adsorption on the surface. An extension of these ideas to spherical nanoparticles at interfaces was done by Aveyard and Clint [15] (see the free energy expression, equation (8)). Figure 4 shows the free energy curves predicted by the thermodynamic model for different values of line tension. The thermodynamic model predicts three different scenarios depending on the magnitude of the line tension; stable, metastable and unstable states. It indicates that the activation energies associated with particle removal from the interface can be relatively low in the presence of the line tension. As a matter of fact, for a line tension of 10^{-11} N, which is of the order expected from theory and simulation studies [33, 16], the activation energy would be around 5 $k_B T$ for a particle of $\approx$1.7 nm radius. The order of magnitude of the activation energy points to the growing importance of fluctuations at the nanometer scale, which should become more relevant as the dimensions of the nanoparticle decrease. Recent computer simulations of nanoparticles at liquid–vapor interfaces by Bresme *et al* [16] have shown that very small nanoparticles of the order of 0.5 nm radius are unstable at liquid–vapor interfaces. In these cases the line tension was negative, therefore it stabilized the particle at the interface by increasing the three-phase line length.

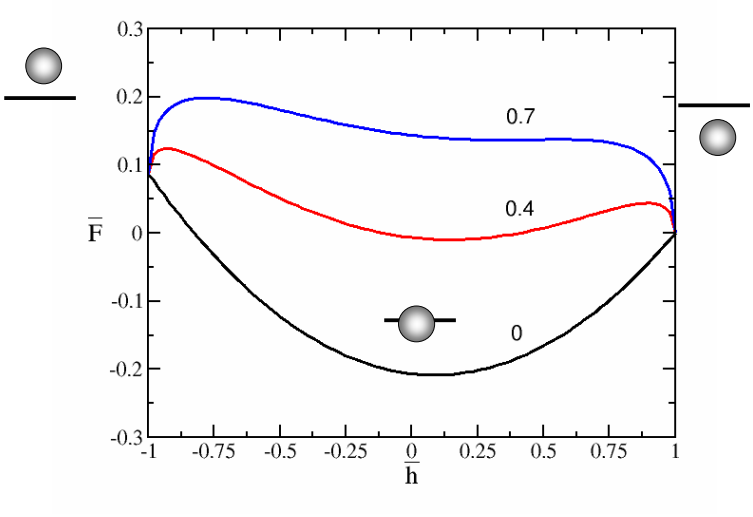

Figure 4. Free energy of a nanoparticle at a fluid interface as a function of nanoparticle immersion. The data correspond to a contact angle of 85° and line tensions $\tau/\gamma_{lv}R = 0$ (stable), 0.4 (metastable), 0.7 (unstable).

Lin *et al* [13, 55] have also suggested that thermal fluctuations can result in a weak interfacial segregation of the nanoparticles at liquid–liquid interfaces. As the particles approach nanometer size the thermal energy becomes comparable to the interfacial energy. In a series of experiments they considered CdSe nanoparticles of diameter 2.7/2.8 nm and 4.6 nm adsorbed at the toluene–water interface and size dependent adsorption and desorption was observed. This effect gives rise to a two-dimensional phase separation at the interface. Considering typical estimates for particle–oil and particle–water surface tensions: 15 and 40 mN m^{-1} respectively, and the oil–water surface tension, 35.7 mN m^{-1}, one can estimate that the activation energy for the detachment of the small particles is about $5k_BT$. This small energy gives rise to a thermally activated escape. The actual value that was inferred from the experiment is in good agreement with the thermodynamic model predictions. Furthermore, consistently with the thermodynamic model the smaller particles have been observed to be less stable than the larger ones and consequently were replaced by those at the interface. The time t associated with particle desorption is expected to follow the following expression, $t = A\exp(-\Delta E/k_BT)$. The adsorption energy, ΔE, increases with the square of the particle radius, indicating that the residence time of the nanoparticles will increase exponentially with particle size. In fact it was found that the 4.6 nm particles assembled at the water–toluene interfaces were stable for days whereas the 2.7 nm particles coalesced within hours due to desorption [55].

The stability of charged nanoparticles at the water–oil interface has also been considered in other experiments [56]. Using nanometer-sized carboxilic acid functionalized gold and CdTe nanoparticles with sizes smaller than 10 nm, it was shown that the nanoparticle adsorption can be regulated by modifying the pH value of the solution. The reversibility observed in this system points to the adequacy of a thermodynamic description of the interfacial stability of the nanoparticles. Reincke and co-workers observed [56] that upon addition of ethanol the contact angle of the gold nanoparticles approaches 90°, resulting in maximum stability at the interface. Wetting experiments have indicated that a contact angle of approximately 90° is required to form stable gold and silver nanoparticle monolayers [57], consistent with the maximum activation energy for detachment inferred from the thermodynamic model.

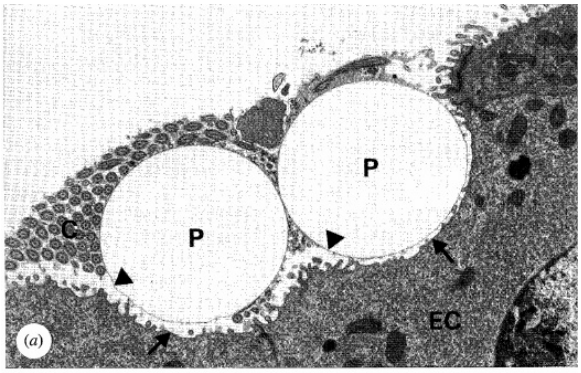

Figure 5. Transmission electron micrograph of the airway epithelium of a hamster. Two polystyrene particles 6 μm diameter are deposited on the airway wall. Reprinted figure with permission from Gehr *et al* [30]. Copyright 2000 The Royal Society.

The thermodynamic model has also been employed to investigate the behavior of small particles in biological tissues (see figure 5). This is a problem of considerable importance in nanotoxicology, with respect to the possible entrapment of very small particles in pulmonary airways. Besides the surface tension of the nanoparticles, line tension effects have also been considered [58]. The stability of biomolecules at fluid interfaces has also been studied by Russel *et al* [59], who investigated the 30 nm diameter cow pea mosaic virus at the perfluorodecalin–water interface (liquid–liquid). The experiments indicated that the virus is stable at the interface.

An extension of the thermodynamic model to particles with heterogeneous wettability, *Janus particles*, has been considered recently [60]. It was predicted that Janus particles, which unlike homogeneous particles are amphiphilic, do exhibit enhanced stability at the interface. The expected maximum desorption energy of nanoparticles of radius $\approx$10 nm at an oil–water interface ($\gamma_{\text{oil-water}} = 36$ mN m^{-1}) is of the order of $10^3\ k_{\text{B}}T$. This result could suggest a route to diminish the effect of thermal fluctuations in experiments dealing with self-assembly of nanoparticle monolayers at interfaces.

3.2. Nonspherical nanoparticles at interfaces

The investigation of nonspherical particles represents a current challenge in the area of nanoparticles at interfaces. This is due in part to the difficulty in manufacturing nanoparticles of specific anisotropic shapes. Recent advances in materials science have provided new routes to produce ellipsoidal and disc-like particles [61–64, 10, 65]. These methods are mostly applicable to microparticles and the production of nanometer ellipsoids with specific aspect ratios remains a challenge in nanomaterials research. Nonetheless, methods for synthesizing particles with some anisotropic shape have been reported [66–69]. These anisotropic nanoparticles should play an important role in testing the predictions and applicability of thermodynamic models at the nanoscale, but systematic studies are still lacking.

The thermodynamic model for prolate/oblate particles at interfaces [17, 70] has been introduced in section 2, see the free energy expression, equations (10) and (11). According to this, it is predicted that the stability of nanoparticles at fluid interfaces is strongly dependent on the particle geometry; in particular, particles with an aspect ratio α larger than a critical value are not stable at the interface. Figure 6(a) shows the impact of the particle geometry on the free

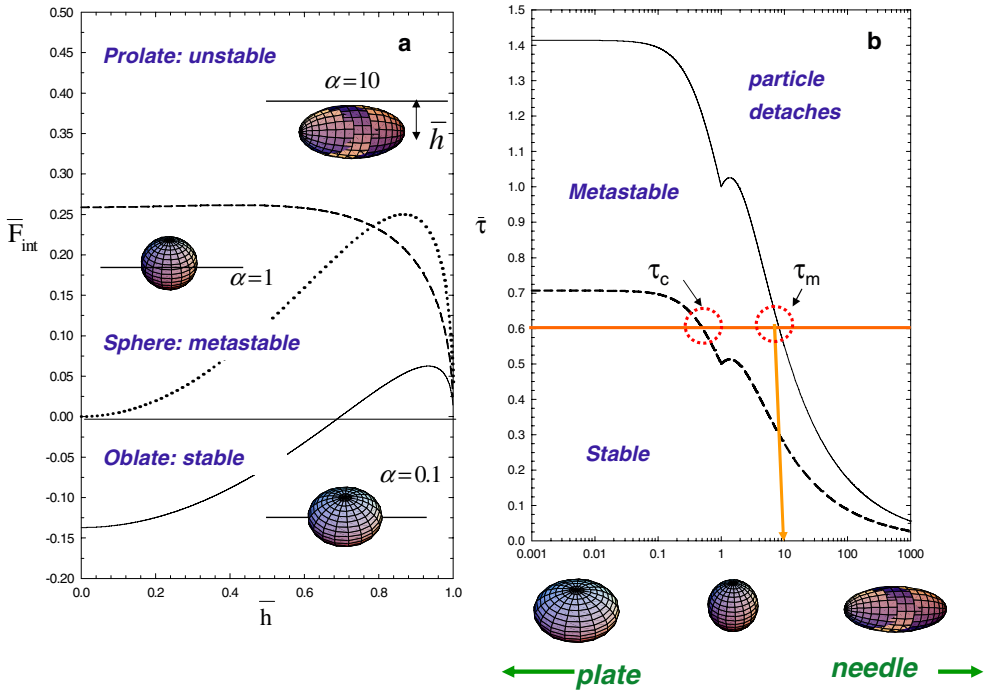

Figure 6. (a) Free energy of nanoparticles at a fluid interface. $\overline{\tau} = 0.6$ ($\approx 10^{-10}$ N for a nanoparticle of radius 10 nm) and $\gamma_{p1} = \gamma_{p2}$. α is the particle aspect ratio, $\alpha < 1$ corresponds to oblate particles (discs), $\alpha = 1$ spheres, and $\alpha > 1$ prolate particles (fibers, needles). (b) Stability diagram of nonspherical particles at fluid interfaces, $\gamma_{p1} = \gamma_{p2}$. The arrow indicate that for a line tension of $\overline{\tau} = 0.6$, nanoparticles with aspect ratio ≈ 10 would detach from the interface [17].

energy of three nanoparticles with the same surface area but different shapes. For a line tension of the order of 10^{-10} N and nanoparticle sizes of ≈ 10 nm size, only oblate-shaped particles would be stable at a water–air interface ($\gamma_{12} = 72$ mN m^{-1}). Spherical nanoparticles would be metastable and prolate particles would be completely unstable, detaching from the interface. According to the general stability diagram of figure 6(b) the increased instability of elongated nanoparticles over spherical and oblate particles persists for other choices of (positive) line tensions. The stability is strongly dependent on the nanoparticle orientation as well (see figure 7). Also the theory indicates that the line tension effects are more important in elongated objects such as nanotubes, nanorods or some biomolecules (viruses). These nanoparticles might prove ideal to investigate experimentally the magnitude of the line tension, given the limited applicability of line tension experiments with microparticles to the nanodomain as discussed in section 2.2.

Recent experimental and molecular modeling investigations have considered 2–5 nm diameter overbased detergent particles [71]. Oblate particles at the interface result in higher values of the surface pressure at close packing as compared with prolate ellipsoids. These results are consistent with the enhanced stability predicted by the thermodynamic model discussed above.

The stability of inorganic nanorods ($BaCrO_4$) with 20 nm length and 5 nm diameter at the water–air interface has been demonstrated recently [72]. Guided by the stability diagram of figure 6, the fact that the rods are stable at the interface implies that the line tension associated to the rod–water–air three-phase line is lower than $+10^{-10}$ N or negative. This is roughly in

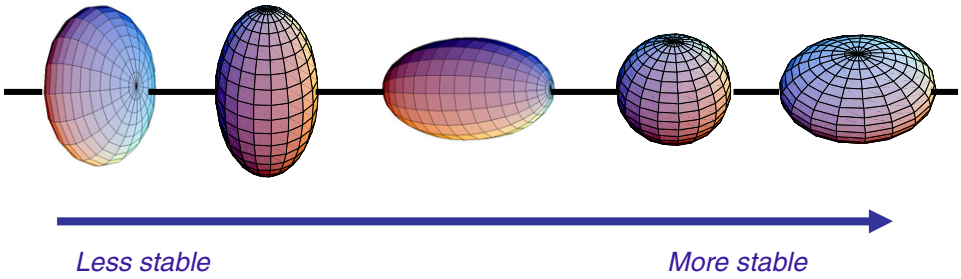

Figure 7. Relative stability of nonspherical nanoparticles at fluid interfaces depending on the particle shape and orientation.

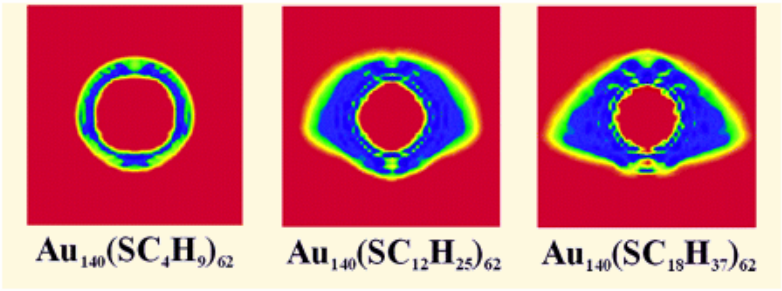

Figure 8. Average density profile of gold passivated nanoparticles adsorbed at the water–air interface. Reprinted with permission from [54]. Copyright 2006 American Chemical Society.

line with the line tensions expected from theory or computer simulations (10^{-12}–10^{-11} N, see the discussion in section 2.2). Regarding other anisotropic particles such as nanotubes, the formation of pure carbon nanotube monolayers at the air–water interface represents a major challenge. Nonetheless, it has been reported that coating the nanotube with a polystyrene salt results in tubes that are partially hydrophilic, stabilizing them at the interface [73]. The aspect ratio of the nanotubes can be very large ($\alpha \gg 100$), according to our previous considerations this might imply that the line tension is either negligible or negative. More experiments in that direction are needed, however, to arrive at more precise statements on the line tension of the nanotube–water–air interface. The stability of disc-shaped nanoparticles at fluid interfaces has also been illustrated in experiments of Laponite discs (30 nm $\times$ 1 nm) adsorbed at the toluene–water interface which are relevant in the stability of Pickering emulsions [74]. According to the thermodynamic model this shape is the one that results in stronger adsorption at interfaces.

Very recently the stability of realistic models of 3 nm gold passivated nanocrystals at the air–water interface has been investigated using molecular dynamics simulations [54]. This study has provided the first microscopic image of the structure of these interfacially trapped nanoparticles. The shape of the particles is strongly influenced by the length of the passivating layer (see figure 8), which determines whether the particles adopt a roughly spherical shape or rather a lens shape. All the nanoparticles investigated were found to be stable at the air–water interface. They had characteristic contact angles, between 70° and 97° for the nanoparticle–air suprasurface contact angle and between 115° and 140° for the subsurface contact angle. The description of the wetting behavior of these particles requires a formulation

of the thermodynamic model that takes into account the 'soft' character of the nanoparticle passivated layer.

Besides nanoparticles with soft coatings, liquid enclosures at interfaces form lens-shaped nanoparticles. The thermodynamics of a drop entry at interfaces has been considered before [3]. Mainly, the stability of liquid 'particles' is determined by the spreading coefficient, S,

$$S = \gamma_{12} - (\gamma_{1p} + \gamma_{2p}). \tag{15}$$

This coefficient must be positive to avoid spreading of the droplet on the interface. Most experiments on liquid droplets at the nanoscale have considered the situation of a droplet on a substrate [44]. On the other hand the stability of 5 nm nanolenses at liquid–liquid interfaces has been investigated via molecular dynamics simulation [75] showing that the Neumann construction [33] very accurately predicts the wetting behavior of these small liquid particles. Also the pressure inside the lens was consistent with the result predicted by Laplace's equation. Overall this investigation showed that macroscopic approaches are very accurate in the description of very small interfaces, similar to the characteristics of the solid, structureless nanoparticles [16] discussed before.

3.3. Nucleation at fluid interfaces

There are many problem of technological interest that are concerned with nucleation processes at fluid interfaces. For example electrodeposition [76] is a process in which metal particles nucleate at a liquid–liquid interfaces under the action of an external electric field. This method has been used to synthesize nanoparticles at liquid–liquid interfaces [77]. Johans *et al* [78] have applied the thermodynamic model described in section 2 to investigate the feasibility of nucleation of metal nanoparticles at liquid–liquid interfaces via electrodeposition experiments. As expected, the surface activity (mainly controlled by the interfacial tensions) of the small nucleus is important in enabling the nucleation process. It was found that nucleation kinetics of palladium at liquid–liquid interfaces was slowed down upon adding surfactant (DOPC), thus reducing the surface tension. This was interpreted as being consistent with the expectations from the thermodynamic model.

Another problem concerned with nucleation at fluid interfaces is the formation of lenticular nuclei from insoluble monolayers. This issue has been investigated by Retter and Vollhardt [79]. Using classical nucleation theory an expression for the free energy of formation of a critical nucleus at an interface was derived. The critical nucleus is strictly speaking a nanoparticle entity with a typical radius of the order of 2–3 nm and its Gibbs free energy is connected to the thermodynamic model discussed before,

$$\Delta G(n) = n\Delta G_\infty + \gamma_{p1}A_{p1} + \gamma_{p2}A_{p2} - \gamma_{12}A_{12} + \tau L \tag{16}$$

where ΔG_∞ is the negative of the supersaturation, n the number of atoms or molecules involved in the cluster and L is the circumference of the nucleus growing at the interface. The free energy of formation shows an explicit dependence with the line tension. From the nucleation of methyl stearate at the air–water interface, line tension values of the order of 10^{-11} N have been estimated [80].

4. Self-assembly of nanoparticles at fluid interfaces

The investigation of nanoparticle self-assembly at fluid interfaces has attracted a significant number of works [81] driven by the motivation to control the preparation of well-characterized films of metallic, semiconducting, magnetic and ferroelectric nanoparticles, which are finding

important applications in advanced materials with specific properties; mechanical, optical or magnetic [1]. Compared to other techniques such as deposition where the film is strongly dependent on the substrate topology, assembly at fluid interfaces proceeds through a rapid exploration of free energy minima owing to the softness and defect-free nature of fluid films.

One major challenge in the self-assembly at fluid interfaces is to control the structure of the resulting aggregate. In the literature, various self-assembled structures at fluid interfaces have been reported, whose origin defies our current understanding of colloidal forces. In the following we review work on nanoparticle self-assembly, classifying the various studies in terms of the nature of the particles; sterically stabilized particles (neutral), charged particles and magnetic particles.

4.1. Sterically stabilized nanoparticles—neutral

Many experiments dealing with sterically stabilized nanoparticles have been performed using metallic quantum dots [82–84]. These nanoparticles consist of a crystalline core of typically 100–300 atoms passivated with alkylthiol layers which make the particles partially hydrophobic and stabilize them at the air–water interface. Array formation for such passivated nanoparticles has been discussed by Gelbart *et al* [18] where it is pointed out that the ratio of metal core radius to passivating layer length to a great extent determines the morphology of the self-assembled structures. A comprehensive investigation of the phase behavior of 2D monolayers of passivated gold and silver nanoparticles (2–7.5 nm diameter) at the air–water interface has been reported by Heath *et al* [85]. Different types of structures were obtained as a function of the volume available to the passivating molecules. Large volumes result in low density monolayers that form 2D foams when compressed. Small volumes on the other hand result in fractal aggregates similar to those obtained from diffusion-limited aggregation, whereas for intermediate volumes, 2D hexagonal phases are obtained. The structural changes undergone by the monolayers as a function of the packing fraction have a strong impact on the collective electrostatic response of the array. It has been reported that silver quantum dot monolayers undergo a metal–insulator transition upon monolayer compression in a Langmuir trough [86]. On the other hand, investigations of polydisperse systems have reported size segregation effects with nanoparticles of the same size tending to group together [87, 88]. This effect has been explained in terms of the size dependence of van der Waals interactions between the particles [88], which is large enough to drive size segregation. Thus, monodispersity is an important requirement for the formation of high quality crystalline arrays.

Experiments have also provided evidence for the formation of exotic nanoparticle structures. Metal nanoparticles (4–6 nm diameter) form circles and linear chains at the air–water interface [18]. It has been argued that these structures are interconnected and that the effect of increasing the nanoparticle concentration is to drive the formation of stripes from circles and networks from linear chains. For a small ratio of passivating layer length to core radius, circular islands are favored, whereas for a large ratio stripes are formed (see figure 1). In the latter case the anisotropy needed to form chains is commonly assigned to interdigitation effects. Computer simulations offer contrasting evidence for interdigitation of ligand shells though [89, 90]. In line with experimental results, the simulations confirm the dependence of the self-assembled structures on the ratio of passivating layer length to core radius. At low packing fractions, nanoparticles passivated with short surfactant layers (butanethiols) form open structures, with local order corresponding to hexagonal packing. For the same core size, longer surfactants (dodecanethiol) give rise to more compact structures exhibiting a change in the crystal symmetry from hexagonal to a distorted square lattice (see figure 9). Similar symmetry changes have been reported in three-dimensional arrays [89].

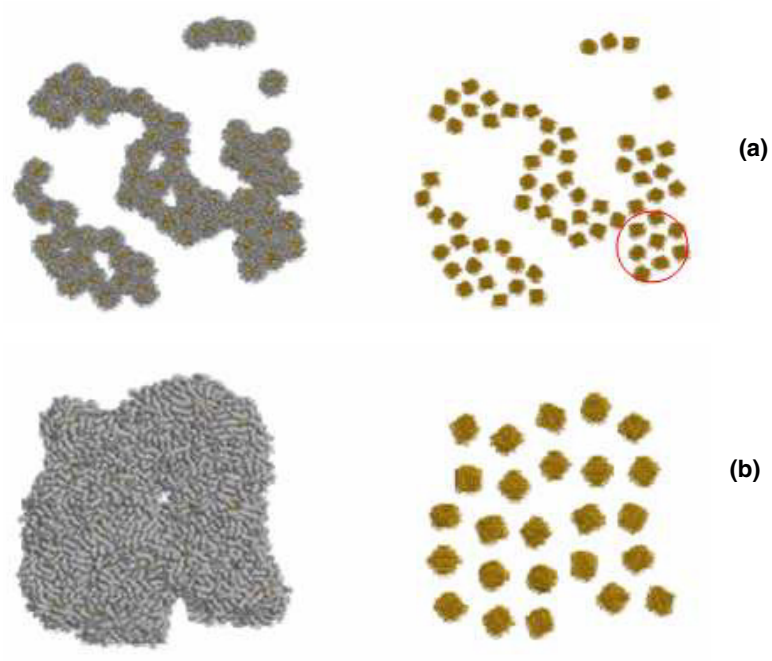

Figure 9. (a) Two-dimensional array of butanethiol nanoparticles. Figures represent the array with (left) and without (right) the passivating layer. The formation of hexagonal lattice has been highlighted. (b) Array of dodecanethiol nanoparticles [90].

The formation of the circular nanoparticle structures discussed above suggests the existence of longer ranged repulsive interactions that limit the cluster size. In [19] it was suggested that the repulsive interactions are connected to electric dipole–dipole interactions with the dipoles being formed by aligned water molecules close to the nanoparticle. Computer simulations of realistic particles have indicated that water molecules reorient at the nanoparticle surface giving rise to a local dipole potential [91]. The electrostatic potential due to this water reorientation is of the same order of magnitude as that of the water–air interface [54]. Nonetheless, to the best of our knowledge the dipole potential has not been measured in experiments, thus the actual origin of the repulsive interaction still remains an open question.

Several computer simulation studies of models employing a combination of attractive and longer ranged repulsive contributions in the intercolloidal potential [19, 92–94] can account with more or less success for the anisotropy connected to the formation of nanoparticle chains. Interestingly, stripe structures can also arise from *isotropic repulsive interactions*, when the repulsive pair potential is defined in terms of two characteristic length scales [95]. The physical origin of some of the longer ranged repulsions used in these studies is related to the entropic repulsion resulting from the overlap of nanoparticle surfactant layers, similar to the interaction originally considered by de Gennes in the context of solid surfaces grafted with polymer chains [96]. On the other hand, for the special case of realistic, passivated gold nanoparticles computer simulations have provided more quantitative information on the effective interactions between the particles. In vacuum the interparticle forces are strongly attractive, the main contribution to this attraction coming from the van der Waals interactions between the atoms of the passivating layer [90, 89]. These interactions can nonetheless be strongly modified when the particles are immersed in a solvent [97] and such modification of the van der Waals interactions

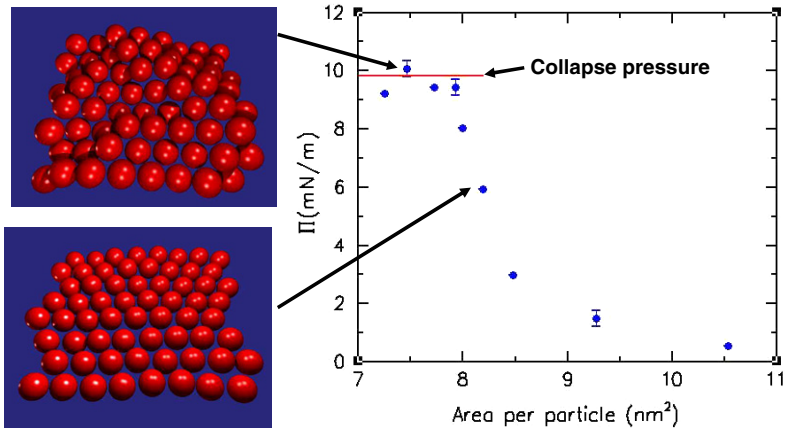

Figure 10. Surface pressure isotherm of nanoparticles (3 nm diameter) at a liquid–vapor interface, computed using molecular dynamics simulations. The solvent is not shown. The snapshots illustrate different stages in the compression process. For pressures beyond the collapse pressure buckling of the monolayer can be observed [51].

in the case of interfacially trapped particles is even more complicated since media with different dielectric constants have to be taken into account in the screening of the van der Waals potential (see section 5).

Besides the formation of clusters and rings, two-dimensional nanoparticle crystals can be assembled which undergo 'buckling' transformations upon compression, characterized by the folding of the monolayer. This effect has been reported in computer simulations [51] (see figure 10) and experiments have confirmed this observation for the case of silver nanoparticles adsorbed at a liquid–liquid interface (water–dichloromethane) [98]. Incidentally, a similar buckling behavior has been observed with latex microparticles at air–water and oil–water interfaces [99], indicating that folding might be a general mechanism that operates in a wide range of length scales.

The importance of thermal fluctuations in the adsorption behavior of nanoparticles at interfaces has been addressed by Lin *et al* [13, 55]. It was observed that in CdSe nanoparticles (1–8 nm) thermal fluctuations result in a weak interfacial segregation at water–toluene interfaces, see also the discussion in section 3.1. This work also indicated that the in-plane diffusion of the nanoparticles is much slower than the one in solution. In a recent article Dai *et al* [100] investigated the self-assembly of dodecanethiol-capped silver nanoparticles (1–5 nm) at the water–trichloroethylene interface. It was suggested they form multilayers instead of a clear monolayer at the interface and that the liquid–liquid interface is very broad with the nanoparticles having no clear preference for either phase. The plausibility of these arguments and thus the origin of these observations is nonetheless unclear. Molecular dynamics simulation of modified hydrocarbon nanoparticles (1.2 nm diameter) at the water–trichloroethylene interface show that this interface has a thickness of molecular dimensions [101]. In this study the particles showed a preference for the hydrophobic phase, and they self-assembled in that phase and not at the interface.

Droplet evaporation as the main nonequilibrium method to induce nanoparticle self-assembly has been investigated by many authors, see e.g. [102–104]. Bigioni *et al* found that the morphology of the assembly formed by gold nanoparticles at a water droplet surface, is mainly controlled by the evaporation kinetics and the particle interactions with the liquid–air

interface [104]. Rapid evaporation and initial formation of two-dimensional islands are needed to obtain extended monolayers in the late stages of drying. Interestingly the islands were found to grow in time both linearly and exponentially, which can be explained considering the diffusion distance traveled by the particles at the interface before they meet an island. The importance of the evaporation rate in driving 2D structures has been addressed in the self-assembly of passivated metal nanoparticles (5.8–7.5 nm diameter) [102]. Fast evaporation of the droplet enables assembly at the droplet liquid–vapor interface whereas slow evaporation conditions favor the nanocrystal diffusion away from the interface and formation of three-dimensional structures.

4.2. Charged nanoparticles

Most studies of charged particles at interfaces have been performed with microparticles owing to their visibility under light microscopes. In the first study of charged polystyrene particle assembly at the water liquid–vapor interface Pieranski [5] reported an electrostatic repulsions between particles, whose range is longer than the electrostatic repulsions in bulk water. This is due to the electric dipoles formed by the colloid surface charge and the counterions, resulting in a power-law dipole–dipole repulsion between the particles, which drives the formation of compact 2D lattices at air–water interfaces (see section 5). Subsequent work using polystyrene particles has investigated the sensitivity of the monolayer structures to electrolyte concentration (water salinity) [105, 99]. At low salinity the repulsion between particles results in fairly ordered arrays. Increasing the salt concentration appears to screen the repulsive interactions and favors irreversible 2D cluster formation. This cluster formation was early addressed by Hurd and Schaefer [106] in investigations of aggregation of silica spheres (300 nm diameter) at the air–water interface. The clusters formed fractal aggregates with a low, characteristic fractal dimension of $\approx$1.2, consistent with the formation of string-like structures at the interface. The tendency to form these structures was rationalized in terms of the energy difference between a particle approaching a dimer from the end and from the side. Larger fractal dimensions ($\approx$1.47–1.58) have been observed for polystyrene particles at the oil–water interface [108] and the induction time for cluster formation upon addition of salt and surfactant has been investigated. The addition of salt alone induces cluster formation only after several days (pointing to a still sizable electrostatic barrier) whereas in combination with surfactants the induction time can be reduced to less than 1 h. It is important to recall that similar fractal aggregates have also been observed in gold nanoparticle experiments (see section 4.1).

The marked insensitivity of very ordered 2D crystal structures of particles at the oil–water interface to salt concentration [99, 107, 108], has been interpreted in terms of likewise dipolar repulsions with no salinity dependence, caused by small residual charges at the particle–oil interface [109, 107]. However, the use of linear screening theory (which for charges present only at the colloid–water surface predicts a strong decrease of the repulsions with increasing salt concentration, see equation (17) below) for interpreting the experiments as done in [99, 107] is hazardous, considering the high charge densities on the water side ($\sim 1e$ nm^{-2}). Nonlinear theory predicts a drastic reduction of the salinity dependence of the electrostatic repulsions [110] (see equation (19) below), however, the absolute magnitude of the observed repulsions still points to additional charges on the oil side beside the ones on the water side [110, 111].

In a series of papers it has been reported that micrometer-size polystyrene particles form mesostructures of circular, chain and soap-froth type at the air–water interface [112, 113, 20, 25] (see figure 11) indicating the possible existence of an attractive minimum in the intercolloidal potential at distances of a few colloid radii. As an alternative

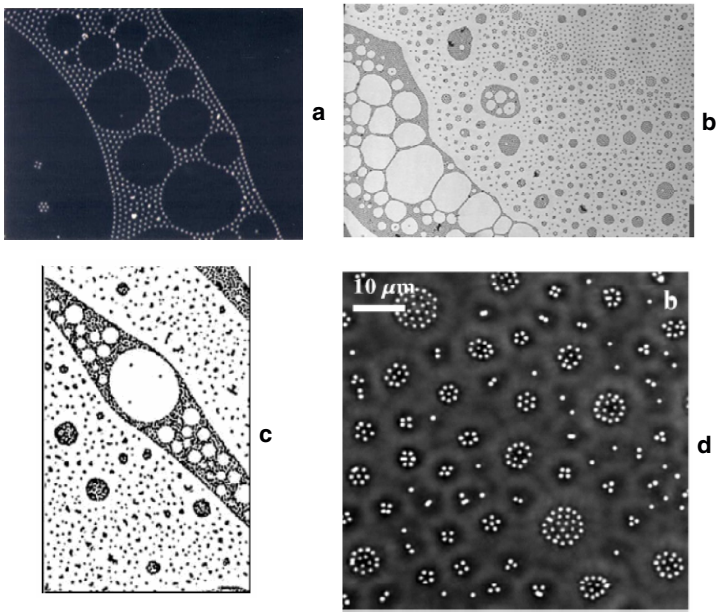

Figure 11. (a) Polystyrene particle arrays formed at the water–air interface. Reprinted with permission from Ruiz-Garcia *et al* [20]. Copyright 1998 by The American Physical Society. (b) Reprinted with permission from Ghezzi and Earnshaw [113]. Copyright 1997 Institute of Physics. (c) Structure formed at a water–air interface contaminated with silicone oil. Reprinted figure with permission from Fernández-Toledano *et al* [115]. Copyright 2004 American Chemical Society. (d) Reprinted figure with permission from Chen *et al* [119]. Copyright 2006 by The American Physical Society.

explanation, different authors [114–116] have suggested that such structures could be explained by oil contamination of the interface. In recent work [117–119] care has been exercised to avoid surface contaminations, yet the colloids still formed small clusters with the particles being well separated, consistent with the original assumption of a longer ranged attractive component in the potential. Stamou *et al* [25] suggested that the attractive contribution could be due to a rugged three-phase contact line which results in the distortion of the air–water interface and induces anisotropic capillary forces between the colloids. Such a rugged contact line could be due to surface roughness, and for sizable capillary attractions between microparticles, the lateral separation between 'hills' and 'valleys' on the colloid surface needs to be on the order of several 100 nm (see equation (25) below). However, electron micrographs of the surface of a polystyrene colloid indicate typical distances between elevations and valley much smaller than that [49]. Another type of heterogeneity on the colloid surface has been demonstrated in [118, 119]. An atomic force microscopy analysis of the distribution of dissociable groups on the colloids showed domains with sizes of the order of 100 nm, indicating that the charge distribution upon immersion in water will be spatially heterogeneous. Through a likewise asymmetric screening cloud, attractive effects in the potential may be expected, however, the theoretical model presented in [119] is not applicable since it is based on the picture that the effective dipole moment of the colloid possesses also a component parallel to the interface plane when the colloid orientation is fluctuating around equilibrium. However, it can be shown that for an arbitrary surface charge distribution (and hence for arbitrary orientation of the colloid) the counterions arrange such that the net dipole moment is always perpendicular to

the interface [120]. Possible attractions arise in higher multipoles; their quantitative effect deserve further consideration. In [121] the possible existence of an attractive minimum between like charged colloids was deduced from the quantitative analysis of a metastable, hexagonal seven-particle cluster of poly(methyl methacrylate) particles at an oil–water interface. It was concluded that the interface deformation induced by the particles was responsible for a capillary interaction that varies logarithmically with distance. This interpretation has been criticized in [122] and contradicted in [23, 24]. On general grounds the capillary forces between charged particles vary with the particle distance as $1/d^4$ (see section 5). In summary, the precise origin of the attractive minimum is still a matter of debate.

The work reviewed above shows that the behavior of charged particles at interfaces is a very dynamic area of research with many questions that still remain to be solved. Experiments using small nanoparticles indicate that the forces inferred from experiments at the microscale may also be found at the nanoscale. Experiments on charged metal nanoparticles (10 nm diameter) at the water–oil interface have been reported very recently [123, 57, 56]. It was found that the interface coverage and consequently the self-assembly could be regulated by changing the nanoparticle surface charge [123, 56]. This was discussed in similar terms by Okubo [124], who correlated the surface activity of silica (100–200 nm diameter) and polystyrene nanoparticles (100–200 nm diameter) to their respective surface character (polar and hydrophobic). In an attempt to explain these results, the surface activity of the nanoparticles was modeled using the thermodynamic model supplemented by electrostatic terms, hence following the same lines used to discuss the behavior of micrometer size particles. It appears that this approximation provides a qualitative explanation of the behavior observed in the small 10 nm particle systems.

The relative ease in the formation and study of 2D colloidal crystals at interfaces also allows to study fundamental questions related to the nature of the liquid–solid phase transition in two dimensions (Kosterlitz–Thouless transition). The equation of state for monolayers of 1.0 and 2.9 μm particles adsorbed at the air–water interface has been reported by Armstrong *et al* [125]. The bigger particles exhibited a behavior consistent with the existence of an hexatic phase [126, 127] characterized by short range translational order and quasi-long range bond-orientational order. Interestingly, the smaller particles showed a first order melting transition. It is difficult to rationalize how such small changes in particle size can impart such dramatic change in the phase behavior as invoked by the authors. Later work has provided clearer evidence for the existence of a first order liquid–hexatic phase transition [128]. Computer simulation of colloidal particles confined to a plane, interacting through dipole–dipole interactions have also considered the formation of hexatic phases [129, 8, 130]. These simulations have reported a first order melting transition, and also provided evidence for the formation of hexatic phases. Nonetheless this simulation work ignores some degrees of freedom that might be relevant in the description of particles at interfaces, for instance particle fluctuations in the direction normal to the interface. The importance of particle motion in the third dimension and its relevance to the hexatic and buckling transitions, has been discussed by Zangi and Rice [131]. The main conclusion form these and other studies [51] is that an appropriate modeling of nanoparticles at interfaces requires the modeling of particle motion in the third dimension.

Mutual interactions of nonspherical nanoparticles will be much richer compared to spherical ones and should give rise to more complex self-assembled structures. However, the study of this field is not yet as well developed as the investigation of spherical particles due to the complications in manufacturing anisotropic shapes in a controlled manner. One can expect that for small distances the shape immediately influences the van der Waals attractions and the steric repulsions. For larger distances, the isotropic electric dipole repulsion will compete with anisotropic capillary forces. For micrometer ellipsoids the latter appear to dominate

the structure formation altogether, as experiments with stretched polystyrene particles (with strong tendency to assemble tip to tip) on the air–water interface show [10, 132]. In the compression of such ellipsoidal monolayers a complicated sequence of buckling and flipping transitions is observed which sets in at much smaller than close packed 2D densities [133]. Recently, the pattern formation of polyelectrolyte/nanotube complexes has been investigated experimentally [73]. These carbon nanotube complexes are stable at the air–water interface and form nematic-like structures, soap froths, rings and cumuli-like structures at different surface pressures. The formation of rings has been explained as a result of competition between the elastic and interfacial energies of the nanotubes. Investigations of $BaCrO_4$ nanorod (20×5 nm) monolayers [72] have also shown a number of structural changes upon compression in a Langmuir trough. Pressure induced isotropic–nematic–smectic transitions were reported. The existence of nematic order is in contrast with the phase diagram of a pure hard rod system [134] for which only isotropic–smectic transition have been observed when the aspect ratio is smaller than 7.

4.3. Magnetic particles

Magnetic particles are starting to attract some attention in the scientific community. This in part is connected to the availability of synthetic methods that enable the making of high quality magnetic nanoparticles. Examples of successful routes to manufacture 13 nm Fe_3O_4 magnetic nanoparticles have been reported [135]. The compression of nanoparticle films result in the formation of circular domains as well as close packed arrays for high surface pressures. Experiments with similar magnetic nanoparticles, γFe_2O_3 (7.5–15.5 nm in diameter) at the air–water interface [136] have reported the formation of chains and compact circular aggregates, reminiscent of the aggregates observed in both neutral and charged particles. These experimental observations have been interpreted in terms of a balance between van der Waals and magnetic dipole–dipole interactions. Preliminary results under the action of a magnetic field [136] indicate that the interactions with the external field are important for field strengths larger than 100 mT.

Magnetic microcolloids adsorbed at the air–water interface have also been used to address the fundamental questions concerning 2D phase transitions. Zahn and Maret [6] investigated the dynamic behavior of a 2D crystal at melting where the crystal consisted of superparamagnetic particles (4.5 μm). In contrast to most other studies with interfacially trapped particles the colloids here were fully wetting and thus did not penetrate the interface but became stabilized near the interface through balancing gravitational weight with repulsive Hamaker forces. A similar method to trap fully hydrophobic, charged particles near water interfaces is presented in [137]. Notably the experimental results were in agreement with the KTHNY theory [126, 127]. These studies were extended to binary mixtures of superparamagnetic colloidal particles [138]. The observed partial clustering (with the small particles in clusters and the big particles left unclustered) was explained in terms of negative nonadditivity in the interactions.

Computer simulations are playing an increasingly important role also in the investigation of two-dimensional magnetic systems. Froltsov *et al* [139] have investigated superparamagnetic suspensions confined to a planar liquid–gas interface and exposed to an external magnetic field. The mutual interaction in these model studies was controlled by magnetic dipole–dipole interactions. The tilt angle of the magnetic moment can be used to control the symmetry of the two-dimensional lattice. Very recently a combined theoretical and simulation study has considered magnetic nanoparticles of ellipsoidal shape at a liquid–liquid interfaces [34, 35]. According to this study, the application of an external field can reorient

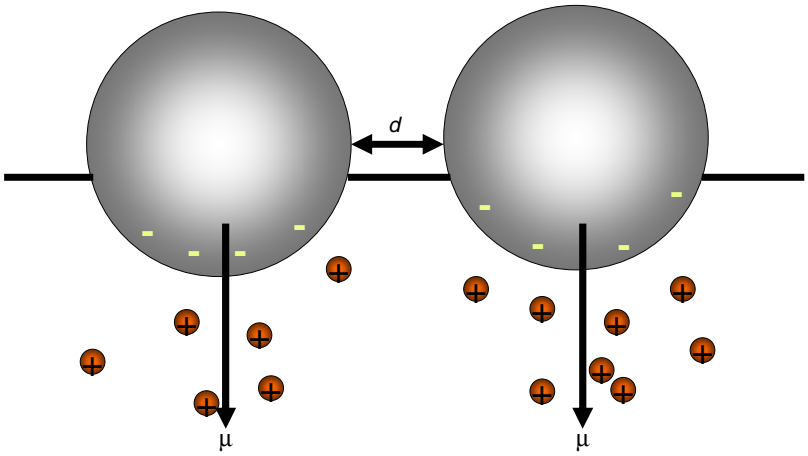

Figure 12. Sketch of two nanoparticles adsorbed at the water–air interface. The asymmetry in the ion cloud gives rise to an electrical dipole moment, μ.

nonspherical nanoparticle at the interface, but the change in orientation features a discontinuous jump that indicates a possible orientational transition at a specific field strength.

5. Forces between nanoparticles at fluid interfaces

The experimental studies of nanoparticles at interfaces have shown a rather complex phenomenology. There is a significant number of works that have proposed theoretical approaches to explain this complex physical behavior. In the following we review the current state of the art on modeling the interactions between particles at interfaces.

5.1. Electrostatic interactions

The electrostatic interaction between charged colloidal particles adsorbed at water interfaces with nonpolar media become strongly modified compared to their interaction in bulk water which is of screened exponential type. Usually, the colloid surface is covered with dissociable groups which release ions when brought in contact with water, resulting in highly charged colloid–water surfaces. However, when the nonpolar medium is oil, residual charges may settle on the colloid–oil surface [107]. In both cases, the effective electrostatic interaction between the colloids is of dipole–dipole type for large distances. In case of the highly charged colloid–water surface, the dipole is formed by the surface charges and the counterions in water (see the discussion below), in case of the charged colloid–oil surface (where the charges reside at a finite distance from the interface) the dipole is formed by the surface charges and their image charge in water.

In a simple model studied by Stillinger [140] and Hurd [141] (colloids are taken as point charges right at the interface and the water phase is treated within linearized Poisson–Boltzmann theory), it was pointed out that in addition to the screened Coulomb repulsive contribution a dipole–dipole interaction was present when particles adsorb at interfaces (see figure 12). The qualitative features of this interaction are expected to be accurate for long intercolloidal distances, where, firstly the potential is smaller than $k_{\mathrm{B}}T$, therefore the linearization becomes a good approximation, and secondly, where the point charge approach is expected to be accurate. However, the strength of the dipole interaction as well as its

dependence on the electrolyte concentration through the Debye screening length κ^{-1}, are subject to strong renormalization [110] of the charge densities on colloid–water surfaces usually encountered in experiment (e.g. $\sigma_c \sim 1e$ nm^{-2} for polystyrene colloids). Also, at short intercolloidal distances (high packing fractions) the nanoparticle–water interface is expected to add a nonnegligible contribution to the electrostatic interactions between these particles [142, 54, 91]. In these cases the molecular nature of water should be considered explicitly.

The (screened) Coulombic and dipole contributions to the interaction energy of two point charges $q = Ze = \sigma_c A$ (A is the colloid surface area exposed to water and σ_c the surface charge density) within the linearized Poisson–Boltzmann equation are given by [141]:

$$U_{\text{dipole}} \propto 2\left(\frac{Ze}{\epsilon\kappa}\right)^2 \frac{1}{d^3} \propto \frac{1}{\epsilon}\frac{\sigma_c^2\kappa^{-2}}{d^3} \qquad (\kappa d > 10) \tag{17}$$

(linear screening)

$$U_{\text{Coulomb}} \propto 2\left(\frac{(Ze)^2}{\epsilon d}\right)\frac{\epsilon^2}{\epsilon^2 - 1}\exp(-\kappa d) \qquad (\kappa d < 10) \tag{18}$$

where ϵ is the ratio of dielectric constants of the liquid (water) and the nonpolar medium, and d is the intercolloidal distance. The effective dipole moment of each particle (as 'seen' in the nonpolar medium) is given by $\mu = Ze\kappa^{-1}/\epsilon$. Hurd showed that above $\kappa r \approx 10$ the interaction is dominated by the dipole–dipole term. For the case of spherical colloids of radius R it has been shown [110] that the squared dependence on the charge density and the screening length of the strength of U_{dipole} is changed to a squared logarithmic one if the nonlinearities in the Poisson–Boltzmann equation are taken into account,

$$U_{\text{dipole}} \sim g\frac{\epsilon_{\text{np}}\epsilon_0}{\beta^2 e^2}\frac{R^4}{d^3}\ln^2(\sigma_c\kappa^{-1}\beta e/\epsilon_w\epsilon_0) \qquad \text{(nonlinear screening)}. \tag{19}$$

Here, ϵ_{np} and ϵ_w are the dielectric constants of the nonpolar phase and water, respectively, ϵ_0 is the dielectric constant of vacuum and $\beta = 1/(k_B T)$ is the inverse temperature. Furthermore $g = 0(1)$ is a geometry factor depending on the contact angle which determines the position of the colloid interface. It turns out that g is independent of σ_c and weakly depends on κ^{-1}; furthermore this implies that the renormalized form of the dipole interaction (19) should be valid for colloids of more or less arbitrary shape, as long as κ^{-1} is smaller than the colloid size.

Very recently it has been demonstrated experimentally that the charge distribution on the particles might be quite inhomogeneous [119]. This inhomogeneity result in anisotropies of the electrostatic interaction in the interface plane. However, it can be shown that for large distances the isotropic dipole repulsion is dominant and possible orientation dependent attractions must be $\propto d^{-4}$. Effects of such inhomogeneous charge distributions on the particle arrays formation might be expected when the screening clouds of two colloids overlap significantly. Further theoretical work is needed to accurately describe this important situation.

Electrostatic forces between colloids are intimately linked to the appearance of electrocapillary interactions due to the deformability of the interface under the action of electrostatic stresses. These implications will be discussed below in section 5.3.

5.2. Van der Waals and short range repulsive interactions

The van der Waals interaction between partially immersed particles is more complicated than that between particles in bulk. This was already noted by Williams and Berg [143] who proposed an extension of the Hamaker treatment to the case of particles at interfaces. This approach can be used to estimate the effective Hamaker constant in terms of the fractional

volume of the particle immersed in the liquid. For a liquid–vapor interface the following equation was derived [143],

$$A_{\text{int}} = A_{\text{vac}} + f^2(3 - 2f)(A_{\text{liquid}} - A_{\text{vac}}) \tag{20}$$

where f is a linear fractional immersion and A_{vac} and A_{liquid}, are the Hamaker constants of the particles in vacuum and in the liquid. This treatment of course ignores the thickness of the interface, and the large changes in density around it (see figure 3), and consequently it is bound to become inaccurate in the case of nanoparticle systems. Nonetheless this simple expression illustrates that van der Waals interactions between particles at liquid–vapor interfaces are expected to be stronger than in the bulk liquid, a point that must be taken into account when interpreting experimental results.

Experiments have provided insight on the dependence of the dispersion interactions with nanoparticle size [88]. In a series of experiments of polydisperse samples of gold nanocrystals capped with dodecanethiol, it was observed that the particles assembled into domains with the larger particles in the center, surrounded by smaller particles. This effect was interpreted in terms of the size dependence of the dispersion interactions. Assuming that the alkylthiol chains have the same dielectric properties as the alkane solvent, the following expression for the interaction between particles of radii R_{A} and R_{B} can be used [144],

$$U_{\text{vdW}}(h) = -\frac{A_{\text{H}}}{12}\left\{\frac{R}{h(1 + h/2(R_{\text{A}} + R_{\text{B}}))} + \frac{1}{1 + h/R + h^2/4R_{\text{A}}R_{\text{B}}} + 2\ln\left(\frac{h(1 + h/2(R_{\text{A}} + R_{\text{B}}))}{R(1 + h/R + h^2/4R_{\text{A}}R_{\text{B}})}\right)\right\} \tag{21}$$

where $h = d - (R_{\text{A}} + R_{\text{B}})$ is the shortest distance between the two particles, A_{H} is the Hamaker constant for gold–gold interactions through dodecane, and $R = 2R_{\text{A}}R_{\text{B}}/(R_{\text{A}} + R_{\text{B}})$. This expression varies as $1/h^6$ for $h \gg R$ similar to a normal $1/d^6$ dispersion interaction, whereas it decays with $1/h$ for $h \ll R$, which corresponds to the limit obtained with the Derjaguin approximation [145].

Computer simulations have suggested that metal passivated nanoparticles interact very strongly through dispersion interactions mediated by the passivating layers. For molecular crystals the interactions are predicted to be of the order of $\approx$150 $k_{\text{B}}T$ [89]. A similar order of magnitude was obtained for passivated nanoparticle pairs in vacuum [90]. Nonetheless it is important to note that the interactions are sensitive to solvent conditions. As a matter of fact, the solvent can strongly modify the Hamaker constant, and screen completely the attractive interactions between nanoparticles in solution [97].

One attempt to get information on the interaction strength between small passivated nanocrystals ($\approx$ 2–4 nm radius) was reported in [146]. The effective pair potential was extracted from small angle x-ray data by means of the hypernetted-chain integral equation. The results were fitted to a potential consisting of a van der Waals contribution, equation (21), and an steric repulsion. The steric repulsion was derived by de Gennes for a tightly packed monolayer in a good solvent [96]. Moreover a Lennard-Jones potential was also considered as effective pair potential. It was concluded that the Lennard-Jones potential adequately fits the experimental results. This suggest that the van der Waals interactions can be well described by an attractive $1/h^6$ interaction. Also it was suggested that the repulsive interactions is short ranged, a feature that is not well described by the steric repulsion in the case small of nanoparticles.

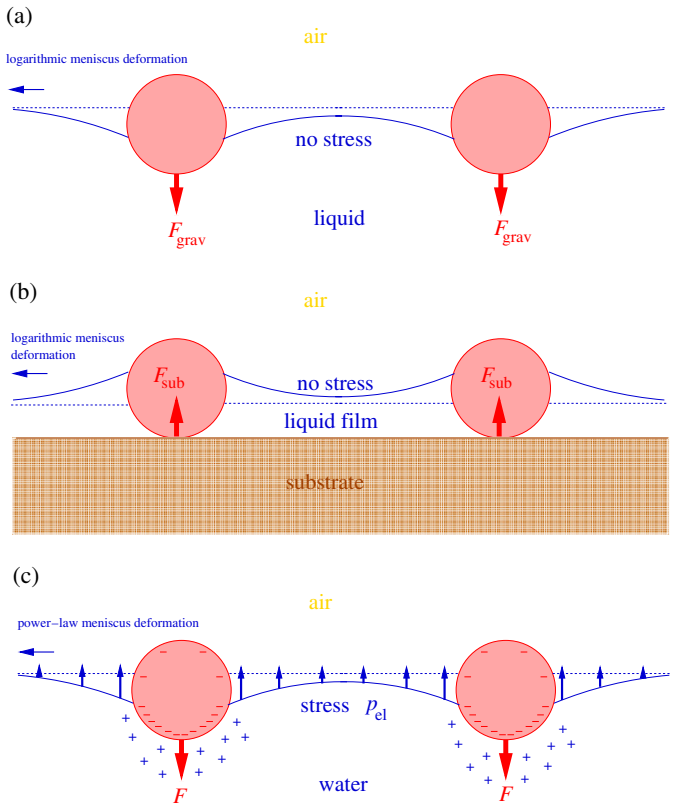

Figure 13. Capillary interactions. (a) Flotation forces: gravity acting on macroparticles causes long ranged, logarithmically varying interface deformations and capillary energies. (b) Immersion forces: microparticles on a substrate covered with a thin film also give rise to logarithmically varying capillary interactions. (c) Freely floating and charged nanoparticles experience capillary interactions of shorter range, $\propto d^{-3}$, due to the combined action of a vertical force on the colloids and an inhomogeneous stress on the interface.

5.3. Capillary forces

Forces isotropic in the interface plane. Capillary forces between small particles have been extensively discussed by Kralchevsky and Nagayama [22], mostly for the case when no stresses act on the interface. In this case, forces on the colloids acting *perpendicular* to the interface result in strong *lateral* forces between particles (which can be attractive or repulsive) due to logarithmic interface (meniscus) deformations (see figure 13(a)). For macroscopic particles, gravity can induce such deformations, causing *flotation forces* whose strength decreases with the sixth power of the particle size. These forces are irrelevant for small particles, $<10\ \mu$m whose dimensions are much smaller than the interface capillary length $\approx$ mm. For these small particles another type of capillary force arises when the particles are adsorbed in a thin film or partially immersed in a liquid. This situation leads to interface perturbation giving rise to *immersion forces*, which again can be attractive if both menisci are concave or convex, or repulsive if one of the meniscus is concave/convex and the other one is convex/concave. These forces result in aggregation across a wide range of length scales, from nanometer to macroscopic scales. For nanoparticles of the same radii, R, partially immersed in a liquid or

in a thin film (see figure 13(b)) the capillary energy as a function of the particle separation d reads [22]

$$U_{\mathrm{cap}} \propto \gamma R^2 K_0(qd) \overset{qd\ll 1}{\rightarrow} -\gamma R^2 \ln(qd) \qquad \text{(immersion)} \tag{22}$$

where γ is the interfacial tension, $K_0(x)$ is the modified Bessel function of zeroth order, $q = \sqrt{(\Delta\rho g - \Pi')/\gamma}$ is the inverse capillary length in thin films, where Π' is the derivative of the disjoining pressure with respect to the film thickness. This expression is valid when the distance between the particles is much smaller than the capillary length ($d \ll q^{-1}$, $q^{-1}_{\mathrm{water}} = 2.7$ mm) and when the radii of the two contact lines is much smaller that the particle separation. The first condition is readily achieved in nanoparticle systems, the second only when particle separation is large enough (low covering). It should be noted that unlike flotation forces, the immersion force increases linearly with the interfacial tension.

Surface charges on colloids may induce capillary effects which go beyond the forces discussed above. In this case the meniscus deformation is caused by the combined effect of a vertical force F acting on the colloid and an inhomogeneous stress field p_{el} acting on the interface, see figure 13(c). This stress field is the difference between the electrostatic stress tensor right above and below the interface. It is very important to distinguish the cases where mechanical isolation holds and where not. Mechanical isolation states that the total force on colloid plus interface is zero ($F = -\int \mathrm{d}A_{\mathrm{men}} p_{\mathrm{el}}$) and the asymptotic meniscus deformation around a single sphere is power-law like, $u(r) \propto r^{-4}$. Mechanical isolation together with the absence of logarithmic meniscus deformations should apply to nanocolloids on a flat interface but it can be shown to hold also for colloids sitting on mesoscopic droplets [147] (for the controversy on this particular case, see [148–150]). The ensuing capillary interaction is attractive and shows a dipole-like decay as does the electrostatic interaction [151, 152],

$$U_{\mathrm{cap}}(d) \sim -\varepsilon_{\mathrm{F}}\, U_{\mathrm{dipole}}(d) \qquad \text{(mechanical isolation)}. \tag{23}$$

Its relative strength compared to the electrostatic dipole repulsion is given by $\varepsilon_{\mathrm{F}} = F/(2\pi\gamma R)$, which is the ratio of the total vertical force acting on the colloid with a force scale set by the surface tension. This ratio must be of order 1 for the capillary attraction to overcome the electrostatic repulsion. As discussed in section 5.1, the colloids may be charged on the nonpolar (oil) side as well as on the water side. On the nonpolar side, charge densities are low [107] ($\sigma_{\mathrm{c}} \sim 10^{-3} e\ \mathrm{nm}^{-2}$), thus $\varepsilon_{\mathrm{F}} \sim \sigma_{\mathrm{c}}^2 R/(\epsilon_{\mathrm{np}}\gamma)$ is small already for microparticles and renders the capillary interaction unimportant for nanoparticles ($\varepsilon_{\mathrm{np}}$ is the dielectric constant of the nonpolar phase). The possibly large colloid charge densities on the water side necessitate to take into account aspects of the full, nonlinear Poisson–Boltzmann problem and yield $\varepsilon_{\mathrm{F}} \sim \sigma_{\mathrm{c}} k_{\mathrm{B}}T/(\gamma e)$ (colloid size independent if the screening length κ^{-1} is smaller than the colloid size), and in this case the capillary attractions can become asymptotically dominant if $\sigma_{\mathrm{c}} \sim 1e\ \mathrm{nm}^{-2}$ and the surface tensions, are low ($\gamma \sim 0.01\ \mathrm{N\,m}^{-1}$, as e.g. for water surfaces treated with surfactant) [151].

Mechanical isolation does not hold if $\Delta F = F + \int \mathrm{d}A_{\mathrm{men}} p_{\mathrm{el}} \neq 0$. Then the asymptotic meniscus deformation $u(r) \propto (\Delta F/\gamma) \ln(qr)$ is logarithmic, as it is the ensuing capillary potential

$$U_{\mathrm{cap}}(d) = \Delta F\, u(d) \propto \frac{(\Delta F)^2}{\gamma} \ln(qd) \qquad \text{(no mechanical isolation)}. \tag{24}$$

The flotation interaction is just a special case where the system is not mechanically isolated ($F = F_{\mathrm{grav}}$, $p_{\mathrm{el}} = 0$). Other examples may be realized when there are external fields acting on the colloids (e.g. laser tweezers).

Forces anisotropic in the interface plane. Colloidal anisotropies may also give rise to meniscus deformations, which result in capillary interactions that are anisotropic themselves. Stamou *et al* [25] have proposed that for spherical colloids the three-phase contact line itself may be wiggly due to surface roughness. In a multipole decomposition of the contact line, the quadrupolar term (with amplitude u_{quad}) causes asymptotically the dominant contribution to the meniscus deformation (monopoles and dipoles must be zero due to force and torque balance). It results in a capillary interaction energy

$$U_{\mathrm{cap}} \sim \gamma\, u_{\mathrm{quad}}^2 \left(\frac{R}{d}\right)^4 \cos(2\phi_1 + 2\phi_2) \qquad \text{(quadrupole interaction)} \qquad (25)$$

where $\phi_{1[2]}$ parametrizes the quadrupole orientation of colloid 1 or 2 in the interface plane. Such an interaction may favor the formation of linear and branched aggregates. Assuming $u_{\mathrm{quad}} \sim R/10$ this capillary force could result in an interaction energy of $10^4\ k_{\mathrm{B}}T$ for 1 μm particles separated by a distance of 2 μm. It would be desirable, however, to gain more insight into the shape of the three-phase contact line using realistic models for the surface roughness of colloidal particles. Undulated contact lines and thus anisotropic capillary forces have been achieved recently with the fabrication of metal and silicon dioxide microparticles [64]. As another example, polymeric ellipsoids have been produced with sizes in the micrometer domain [10]. Their aspect ratio, however, appears to be easily tunable in the range 1–10. For contact angles $\theta \neq 90°$, Young's law necessitates sizable undulations of the contact line, with a leading quadrupole amplitude u_{quad} of several hundred nm, if the aspect ratio is large [10, 132]. According to equation (25), this leads to strong interactions and the resulting surface structure might not necessarily be thermally equilibrated [133]. For small eccentricities, the capillary problem can be solved perturbatively and Langevin simulations of the structure formation result in dendritic or hexagonal-lattice-type structures [153].

5.4. Fluctuation forces

The instantaneous location of a fluid interface between two phases in equilibrium is not fixed but is affected by thermal fluctuations. The resulting deviations $u(\mathbf{r})$ from a certain mean position of the interface are termed capillary waves which are easily excitable. Without damping, capillary waves would completely blur an interface, however damping on a macroscopic length scale is introduced by gravity (associated with the capillary length $\lambda \sim O$ (mm)) or through a finite interface (as e.g. on a droplet). Thermal correlators of capillary waves are long ranged, logarithmic for distances smaller than the capillary length, $\langle u(\mathbf{r})u(0)\rangle \sim (k_{\mathrm{B}}T/\gamma)\ \ln(\lambda/r)$, and the squared width of the interface diverges logarithmically with the capillary length (or the interface size), $\langle u^2(\mathbf{r})\rangle \sim (k_{\mathrm{B}}T/\gamma)\ \ln(\lambda/\sigma)$, where σ is a characteristic atomistic length of the fluid [154]. For atomistic fluids, capillary waves can be probed with x-ray and dynamic light scattering, see e.g. [155, 156], for interfaces of colloidal fluids they have been visualized by videomicroscopy in real space [157].

Colloids trapped on an interface can be viewed as 'obstacles' which restrict the possible fluctuations of the capillary waves through boundary conditions at the three-phase contact line. If two colloids are placed on the interface at mutual distance d, the fluctuation spectrum of capillary waves will depend on d as will the associated free energy of the capillary waves. Thus a distance dependent fluctuation force arises which is a thermal variant of the Casimir effect which was originally discussed in the context of the force induced by quantum fluctuations between two plates in vacuum [158].

General aspects of the Casimir effect associated with thermal Gaussian fluctuations (which capillary waves belong to) have been discussed in [159]. Note that the amplitude of the

corresponding Casimir energies is generically fixed by $k_B T$, thus one would expect that these become more important if one moves from the microcolloidal to the nanocolloidal domain.

The fluctuation potential has two contributions [26, 27]: (i) from the effects of the fluctuating interface itself with the three-phase contact line held at constant, equilibrium position and (ii) from a random motion of the three-phase contact line. The contributions to (ii) can be varied by certain constraints imposed on the colloid which strongly influence the fluctuation energy at large distances (yet smaller than the capillary length). For the example of spherical colloids of radius R ($\theta = 90°$) at distance $d \gg R$, the fluctuation potential is double logarithmic in the distance for *fixed* colloids (e.g. by laser tweezers), whereas it is a weak power law for *freely fluctuating* colloids [26, 27],

$$U_{\text{fluc}} \sim \begin{cases} k_B T \ \ln\ln\left(\dfrac{d}{R}\right) & \text{(fixed colloid)} \\ -k_B T \left(\dfrac{R}{d}\right)^8 & \text{(free colloid).} \end{cases} \tag{26}$$

On the other hand, the potential is independent on the constraints on the colloid when they are close and it is divergent when the surface-to-surface distance $h = d - 2R$ goes to zero:

$$U_{\text{fluc}} = -k_B T \frac{\pi^2}{24}\sqrt{\frac{R}{h}} \qquad (h \to 0). \tag{27}$$

Thus the fluctuation potential is very strong for small separations, similar to the van der Waals potential (which however is stronger, $U_{\text{vdW}} \sim 1/h$ for $h/R \to 0$, see section 5.2). This implies that when the effective Hamaker constant at the interface is small and thus van der Waals forces are weak, the fluctuation force could drive colloidal coagulation.

Anisotropies in the particle shape lead to anisotropies in the fluctuation potential. Note, however, that as for capillary interactions, where logarithmic terms arising from a net force on colloid and interface are always isotropic, the logarithmic terms in the fluctuation potential (caused by fixing the colloid) are isotropic. Thus anisotropic fluctuation interactions are asymptotically dominant only if the colloids are not fixed. The only example treated in the literature is the case of thin rods of length L who experience a potential [160],

$$U_{\text{fluc}} = -\frac{k_B T}{128}\left(\frac{L}{d}\right)^4 \cos^2(\phi_1 + \phi_2) \qquad \text{(thin rods)} \tag{28}$$

where ϕ_i parametrizes the orientation of rod $i = 1$ or 2 in the interface plane.

5.5. Solvation forces

For colloids becoming smaller and their size approaching typical solvent length scales one can expect that molecular details of the solvent and interface structure become important. These molecular details are not captured completely by the mesoscopic type of interactions discussed above. For bulk solvents, the associated solvation forces between colloids [161] have been discussed for various systems, most notably depletion effects in hard body solvents or the chemically and biologically important case of colloids in water. However, there are not at the moment systematic investigations of the solvation forces between nanoparticles at interfaces. Only preliminary studies [162] indicate that the solvation forces are reduced with respect to the forces in the liquid phase, and that exhibit a long range behavior that could be consistent with the fluctuation force associated to the interfacial thermal fluctuations (Casimir effect).

Table 1. Interactions of nanoparticles at fluid interfaces. R denotes the colloid size (e.g. the radius for spherical colloids) and h a distance of closest approach ($h = d - 2R$ for spherical colloids). The interaction potential is generically given by (functionality) $\times$ (strength). The last column indicates the range of particle sizes for which the corresponding interactions are expected to play a significant role.

Interaction	Character	Functionality	Strength (k_BT)	Particle size
Capillary				
–immersion	att/rep	$\ln(R/d)$	$10 \ldots 10^5$	nm... mm
–electrostatic	att	$(R/d)^3$	$1 \ldots 10^3$	100 nm ... μm
–anisotropic	att/rep	$(R/d)^4 f(\phi)$	$1 \ldots 10^5$	μm
Electrostatic				
–dipolar	rep	$(R/d)^3$	$10 \ldots 10^5$	nm ... μm
Van der Waals	att	$(R/h) \ldots (R/d)^6$	$0.1 \ldots 1$	nm ... μm
Fluctuation force				
–fixed colloids	att	$(R/h)^{1/2} \ldots \ln\ln(d/R)$	1	nm
–free colloids	att	$(R/h)^{1/2} \ldots (R/d)^8$	1	nm
Solvation	att/rep/osc		1	nm

5.6. Summary of interactions between particles at interfaces

In table 1 we summarize the properties of the colloidal interactions which may occur at fluid interfaces. Electrostatic and van der Waals interactions have been the cornerstone for discussing colloidal properties in the bulk, and they retain their importance for colloids at interfaces. Here, the presence of the interface introduces an additional dipole character in the electrostatic interactions. Peculiar to colloids at fluid interfaces are capillary interactions. Long-known gravity induced capillary interactions are unimportant for microparticles and nanoparticles but new electrocapillary interactions arise which necessarily accompany the electrostatic dipole repulsions. For nonspherical colloids, the resulting capillary interactions are anisotropic and strong and presumably they will play a major role in the self-assembly of anisotropic nanocolloids.

Capillarity and electrostatics are only marginally affected by thermal fluctuations and may be regarded as 'classical' interactions. On the other hand, fluctuations manifest themselves in the appearance of Casimir-type interactions which should gain importance in the nanocolloidal regime when the 'classical' interactions become smaller. Finally, colloidal interactions connected to molecular details of the fluid interface (solvation forces) represent the least known type of interaction and represent a major challenge for the future.

6. Conclusion

As we attempted to show in this small survey on the research activities concerning nanoparticle behavior near interfaces, this topic is increasingly gaining focus in studies of colloid science. Most of the experimental and theoretical activities that have been reviewed here address basic features of nanoparticle physics at interfaces, with emphasis on qualitative aspects rather than on quantitative details. Nevertheless, a more quantitative characterization is desirable and will become available with the advance of measurement techniques and nanoparticle production technology. The experiments performed in the last decade (especially on self-assembly) point to the possible applicability of interfacially trapped nanoparticles to technological problems as well as to their use as (quasi-)two-dimensional model systems in condensed matter physics. The self-assembly of nanoparticles adsorbed at fluid interfaces, e.g. air–water, can be very

complex as illustrated by the unusual two-dimensional structures observed in experiments. For the purpose of generating structures in a controlled manner, a clear microscopic interpretation of the origin of these structures in terms of molecular interactions is highly wanted and remains a major challenge in colloid science. As discussed in this review the theoretical treatment of nanoparticles at interfaces is far from trivial. Unlike many bulk colloidal suspensions, which can be well characterized in terms of a balance of electrostatic and van der Waals forces, the effective interactions between particles at interfaces include more contributions due to the deformability of the interface as well as due to the inherent discontinuities (density, permittivity) of the interfaces. Interface deformation in particular may play a very important role in the self-assembly of nanoparticles at interface, especially when the particles are complexly shaped or chemically heterogeneous. The disentanglement of the various effective interface forces in experiment should become possible with the availability of methods for the synthesis of nanocolloids with specific shapes and chemical compositions. This, we believe, represents an important challenge for the coming years.

Given the complexity of the interactions of particles at interfaces, the availability of simple, effective theoretical models describing the generic physical behavior of these systems is desirable as well. Macroscopic concepts represent a natural first approach in this sense. Indeed, despite all the complications arising from approaching the molecular scale, it would be useful to understand the stability and also aspects of the intercolloidal forces using the macroscopic concepts of surface and line tension, i.e., gain an understanding on how these quantities are modified on small scales with respect to larger systems. As we summarily showed in this work, there is experimental evidence that these macroscopic ideas can explain the generic stability behavior of particles at interfaces. Additionally, computer simulations of model systems have enabled to test the applicability of macroscopic approaches to nanoparticles adsorbed at interfaces, showing that these can be surprisingly accurate for particles as small as 3 nm in diameter. Moreover, at the time of writing simulations appear to be the quantitatively most reliable tool to predict line tensions (which according to available results span $\approx 10^{-12} \ldots 10^{-11}$ N) and to study stability effects linked to line tension. These predictions ask for experimental confirmation, necessitating the development of experimental methods to accurately measure line tensions and to observe the related effects. The use of standard techniques to measure the line tension is complicated in the case of nanoparticles and at the moment there are none which are able to accurately measure contact angles or line tensions of nanoparticles of a few nanometers diameter. Further in the future, the visualization of interfaces on the molecular scale, in particular the shape of the three-phase line around a nanoparticle, is an important objective as well which would give us immediate access to the understanding of nanoparticle interactions related to interface deformation.

Acknowledgments

FB would like to thank EPSRC and The Royal Society for financial support. He would also like to thank Professor S Dietrich, Dr M Oettel and Mr H Lehle for their hospitality at the Max Planck Institute of Metal Research (Stuttgart) where part of this work was written. MO acknowledges financial support from the German Science Foundation through the Collaborative Research Center 'Colloids in External Fields' (SFB-TR6).

References

[1] Ozin G A and Arsenault A 2005 *Nanochemistry: A Chemical Approach to Nanomaterials* (Cambridge: RSC Publishing)
[2] Fendler J H 1996 *Curr. Opin. Colloid Interface Sci.* **1** 202

[3] Aveyard R and Clint J H 1995 *J. Chem. Soc. Faraday Trans.* **91** 2681
[4] Binks B P 2002 *J. Colloid Interface Sci.* **7** 21
[5] Pieranski P 1980 *Phys. Rev. Lett.* **45** 569
[6] Zahn K and Maret G 2000 *Phys. Rev. Lett.* **85** 3656
[7] Bausch A R, Bowick M J, Cacciuto A, Dinsmore A D, Hsu M F, Nelson D R, Nikolaides M G, Travesset A and Weitz D A 2003 *Science* **299** 1716
[8] Terao T and Nakayama T 1999 *Phys. Rev.* E **60** 7157
[9] Dinsmore A D, Hsu M F, Nikolaides M G, Marquez M, Bausch A R and Weitz D A 2002 *Science* **298** 1006
[10] Loudet J C, Alsayed A M, Zhang J and Yodh A G 2005 *Phys. Rev. Lett.* **94** 018301
[11] Whitesides G M 1997 *Science* **276** 233
[12] Aizenberg J, Braun P V and Wiltzius P 2000 *Phys. Rev. Lett.* **84** 2997
[13] Lin Y, Skaff H, Emrick T, Dinsmore A D and Russell T P 2003 *Science* **299** 226
[14] Gibbs J W 1961 *The Scientific Papers of J Willard Gibbs* vol 1 (Connecticut: Ox Bow Press) p 288
[15] Aveyard R and Clint J H 1996 *J. Chem. Soc. Faraday Trans.* **92** 85
[16] Bresme F and Quirke N 1998 *Phys. Rev. Lett.* **80** 3791
[17] Faraudo J and Bresme F 2003 *J. Chem. Phys.* **118** 6518
[18] Gelbart W G, Sear R P, Heath J R and Chaney S 1999 *Faraday Discuss.* **112** 299
[19] Sear R P, Chung S-W, Markovich G, Gelbart W M and Heath J R 1999 *Phys. Rev.* E **59** R6255
[20] Ruiz-Garcia J, Gomez-Corrales R and Ivelv B I 1998 *Phys. Rev.* E **58** 660
[21] Derjaguin B V and Landau L 1941 *Acta Physicochim. (URSS)* **14** 633
Verwey E J and Overbeek J T G 1948 *Theory of the Stability of Lyophobic Colloids* (Amsterdam: Elsevier)
[22] Kralchevsky P A and Nagayama K 2000 *Adv. Colloid Interface Sci.* **85** 145
[23] Foret L and Würger A 2004 *Phys. Rev. Lett.* **92** 058302
[24] Oettel M, Dominguez A and Dietrich S 2005 *Phys. Rev.* E **71** 051401
[25] Stamou D, Duschl C and Johannsmann D 2000 *Phys. Rev.* E **62** 5263
[26] Lehle H, Oettel M and Dietrich S 2006 *Europhys. Lett.* **75** 174
[27] Lehle H and Oettel M 2007 *Phys. Rev.* E **75** 011602
[28] Kardar M and Golestanian R 1999 *Rev. Mod. Phys.* **71** 1233
[29] Tronin A, Dubrovsky T, Dubrovskaya S, Radicchi G and Nicolini C 1996 *Langmuir* **12** 3272
[30] Gehr P, Geiser M, Im Hof V and Schürch S 2000 *Phil. Trans. R. Soc.* A **358** 2707
[31] Bresme F and Quirke N 1999 *J. Chem. Phys.* **110** 3536
[32] Bresme F and Quirke N 1999 *Phys. Chem. Chem. Phys.* **1** 2149
[33] Rowlinson J S and Widom B 2002 *Molecular Theory of Capillarity* (New York: Dover)
[34] Bresme F and Faraudo J 2007 *J. Phys.: Condens. Matter* **19** 375110
[35] Bresme F 2007 *Eur. Phys. J.* B submitted
[36] Amirfazli A and Neumann A W 2004 *Adv. Colloid Interface Sci.* **110** 121
[37] Drelich J 1996 *Colloids Surf.* A **116** 43
[38] Getta T and Dietrich S 1998 *Phys. Rev.* E **57** 655
[39] Schimmele L, Napiórkowski M and Dietrich S 2007 *Preprint* cond-mat/0703821
[40] Widom B 1995 *J. Phys. C: Solid State Phys.* **99** 2803
[41] Indekeu J O 1992 *Physica* A **183** 439
[42] Szleifer I and Widom B 1992 *Mol. Phys.* **75** 925
[43] Pompe T 2002 *Phys. Rev. Lett.* **89** 076102
[44] Checco A, Guenoun P and Daillant J 2003 *Phys. Rev. Lett.* **91** 186101
[45] Wang J Y, Betelu S and Law B M 1999 *Phys. Rev. Lett.* **83** 3677
[46] Aveyard R, Beake B D and Clint J H 1996 *J. Chem. Soc. Faraday Trans.* **92** 4271
[47] Mingis J and Scheludko A 1979 *J. Chem. Soc. Faraday Trans.* **75** 1
[48] Vinke K, Bierman G, Hamersma P J and Fortuin J M H 1991 *Chem. Eng. Sci.* **46** 2497
[49] Yakubov G E, Vinogradova O W and Butt H J 2000 *J. Adhes. Sci. Technol.* **14** 1783
[50] Aveyard R and Clint J H 1995 *J. Chem. Soc. Faraday Trans.* **91** 175
[51] Fenwick N, Bresme F and Quirke N 2001 *J. Chem. Phys.* **114** 7274
[52] Powell C, Fenwick N, Bresme F and Quirke N 2002 *Colloids Surf.* A **206** 241
[53] Aveyard R, Clint J H and Nees D 2000 *Colloid Polym. Sci.* **278** 155
[54] Tay K A and Bresme F 2006 *J. Am. Chem. Soc.* **128** 14166
[55] Lin Y, Böker A, Skaff H, Cookson D, Dinsmore A D, Emrick T and Russell T P 2005 *Langmuir* **21** 191
[56] Reincke F *et al* 2006 *Phys. Chem. Chem. Phys.* **8** 3828
[57] Duan H, Wang D, Kurth D G and Möhwald H 2004 *Angew. Chem. Int. Edn* **43** 5639

[58] Geiser M, Schürch S, Im Hof V and Gehr P 2000 Retention of particles: structural and interfacial aspects *Particle–Lung Interaction* (*Lung Biology and Health Diseases*) vol 143, exec. ed C Lenfant, ed P Gehr and J Heyder (New York: Dekker) pp 291–322
[59] Russell J T, Lin Y, Boker A, Su L, Carl P, Zettl H, He J B, Sill K, Tangirala R, Emrick T, Littrell K, Thiyagarajan P, Cookson D, Fery A, Wang Q and Russell T P 2005 *Angew. Chem. Int. Edn* **44** 2420
[60] Binks B P and Fletcher P D I 2001 *Langmuir* **17** 4708
[61] Rees G D, Evans-Gowing R, Hammond S J and Robinson B H 1999 *Langmuir* **15** 1993
[62] Ho C C, Keller A, Odell J A and Ottewill R H 1993 *Colloid Polym. Sci.* **271** 469
[63] Snoeks E, van Blaaderen A, van Dillen T, van Kats C M, Brongersma M L and Polman A 2000 *Adv. Mater.* **12** 1511
[64] Brown A B D, Smith C G and Rennie A R 2000 *Phys. Rev.* E **62** 951
[65] Wang H, Brandl D W, Le F, Nordlander P and Halas N J 2006 *Nano Lett.* **6** 827
[66] Tanori J and Pileni S 1997 *Langmuir* **13** 639
[67] Li M, Schnablegger H and Mann S 1999 *Nature* **402** 393
[68] Chang S S, Shih C W, Chen C D, Lai W C and Wang C RC 1999 *Langmuir* **15** 701
[69] Peng X G, Manna L, Yang W D, Wickham J, Scher E, Kadavanich A and Alivisatos A P 2000 *Nature* **404** 59
[70] Faraudo J and Bresme F 2004 *J. Non-Equilib. Thermodyn.* **29** 397
[71] Bearchell C A, Heyes D M, Moreton D J and Taylor S E 2001 *Phys. Chem. Chem. Phys.* **3** 4774
[72] Kim F, Kwan S, Akana J and Yang P 2001 *J. Am. Chem. Soc.* **123** 4360
[73] Hernández-López J L, Alvizo-Páez E R, Moya S R and Ruiz-García J 2006 *J. Phys. Chem.* B **110** 23179
[74] Ashby N P and Binks B P 2000 *Phys. Chem. Chem. Phys.* **2** 5640
[75] Bresme F and Quirke N 2000 *J. Chem. Phys.* **112** 5985
[76] Dryfe R A W 2006 *Phys. Chem. Chem. Phys.* **8** 1869
[77] Cheng Y F and Schiffrin D 1996 *J. Chem. Soc. Faraday Trans.* **92** 3865
[78] Jihans C, Liljeroth P and Kontturi K 2002 *Phys. Chem. Chem. Phys.* **4** 1067
[79] Retter U and Vollhardt D 1993 *Langmuir* **9** 2478
[80] Retter U, Siegler K and Vollhardt D 1996 *Langmuir* **12** 3976
[81] Collier C P, Vossmeyer T and Heath J R 1998 *Annu. Rev. Phys. Chem.* **49** 371
[82] Dabboussi B O, Murray C B, Rubner M F and Bawendi M G 1994 *Chem. Mater.* **6** 216
[83] Whetten R L, Shafigullin M N, Khoury J T, Schaaff T G, Vezmar I, Alvarez M M and Wilkinson A 1999 *Acc. Chem. Res* **32** 397
[84] Daniel M C and Astruc D 2004 *Chem. Rev.* **104** 293
[85] Heath J R, Knobler C M and Leff D V 1997 *J. Phys. Chem.* B **101** 189
[86] Collier C P *et al* 1997 *Science* **277** 1978
[87] Fink J, Brust M, Bethell D and Schiffrin D J 1998 *Nature* **396** 444
[88] Ohara P C, Leff D V, Heath J R and Gelbart W M 1995 *Phys. Rev. Lett.* **75** 3466
[89] Luedtke W D and Landman U 1996 *J. Phys. Chem.* **100** 13323
[90] Tay K and Bresme F 2005 *Mol. Simul.* **31** 515
[91] Tay K and Bresme F 2006 *J. Mater. Chem.* **16** 1956
[92] Imperio A and Reatto L 2004 *J. Phys.: Condens. Matter* **16** S3769
[93] Mossa S, Sciortino F, Tartaglia P and Zaccarelli E 2004 *Langmuir* **20** 10756
[94] Wang J C, Neogi P and Forciniti D 2006 *J. Chem. Phys.* **125** 194717
[95] Malescio G and Pellicane G 2003 *Nat. Mater.* **2** 97
[96] de Gennes P G 1987 *Adv. Colloid Interface Sci.* **27** 189
[97] Patel N and Egorov S A 2007 *J. Chem. Phys.* **126** 054706
[98] Schwartz H, Harel Y and Efrima S 2001 *Langmuir* **17** 3884
[99] Aveyard R, Clint J H, Nees D and Paunov V N 2000 *Langmuir* **16** 1969
[100] Dai L L, Sharma R and Wu C 2005 *Langmuir* **21** 2641
[101] Luo M X, Mazyar O A, Zhu Q, Vaughn M W, Hase W L and Dai L L 2006 *Langmuir* **22** 6385
[102] Narayanan S, Wang J and Lin X-M 2004 *Phys. Rev. Lett.* **93** 135503
[103] Ohara P C, Heath J R and Gelbart W M 1997 *Angew. Chem. Int. Edn* **36** 1078
[104] Bigioni T P, Lin X M, Nguyen T T, Corwin E I, Witten T A and Jaeger H M 2006 *Nat. Mater.* **5** 265
[105] Robinson D J and Earnshaw J C 1993 *Langmuir* **9** 1436
[106] Hurd A J and Schaefer D W 1985 *Phys. Rev. Lett.* **54** 1043
[107] Aveyard R, Binks B P, Clint J H, Fletcher P D I, Horozov T S, Neumann B, Paunov V N, Annesley J, Botchway S W, Nees D, Parker A W, Ward A D and Burgess A N 2002 *Phys. Rev. Lett.* **88** 246102
[108] Reynaert S, Moldenaers P and Vermant J 2006 *Langmuir* **22** 4936
[109] Sun J and Stirner T 2001 *Langmuir* **17** 3103

[110] Frydel D, Dietrich S and Oettel M 2007 *Phys. Rev. Lett.* at press (*Preprint* 0705.1463)
[111] Park B J, Pantina J P, Furst E, Oettel M, Reynaert S and Vermant J 2007 *Langmuir* submitted
[112] Ruiz-Garcia J, Gómez-Corrales R and Ivlev B I 1997 *Physica* A **236** 97
[113] Ghezzi F and Earnshaw J C 1997 *J. Phys.: Condens. Matter* **9** L517
[114] Kralchevsky P A and Denkov D N 2001 *Curr. Opin. Colloid Interface Sci.* **6** 383
[115] Fernandez-Toledano J C, Mocho-Jordá A, Martínez-López F and Hidalgo-Álvarez R 2004 *Langmuir* **20** 6977
[116] Fernandez-Toledano J C, Moncho-Jordá A, Martínez-López F and Hidalgo-Álvarez R 2006 *Langmuir* **22** 6746
[117] Gomez-Guzman O and Ruiz-Garcia J 2005 *J. Colloid Interface Sci.* **291** 1
[118] Chen W, Tan S S, Ng T K, Ford W T and Tong P 2005 *Phys. Rev. Lett.* **95** 218301
[119] Chen W, Tan S S, Huang Z S, Ng T K, Ford W T and Tong P 2006 *Phys. Rev.* E **74** 021406
[120] Oettel M, Frydel D and Dominguez A 2007 *Preprint* 0706.3977
[121] Nikolaides M G, Bausch A R, Hsu M F, Dinsmore A D, Brenner M P, Gay C and Weitz D A 2002 *Nature* **420** 299
[122] Megens M and Aizenberg J 2003 *Nature* **424** 1014
[123] Reincke F, Hickey S G, Kegel W K and Vanmaekelbergh D 2004 *Angew. Chem. Int. Edn* **43** 458
[124] Okubo T 1995 *J. Colloid Interface Sci.* **171** 55
[125] Armstrong A J, Mockler R C and O'Sullivan W J 1989 *J. Phys.: Condens. Matter* **1** 1707
[126] Young A P 1979 *Phys. Rev.* B **19** 1855
[127] Nelson D R and Halperon B I 1979 *Phys. Rev.* B **19** 2457
[128] Marcus A H and Rice S A 1996 *Phys. Rev. Lett.* **77** 2577
[129] Kalia R K and Vashishta P 1981 *J. Phys. C: Solid State Phys.* **14** L643
[130] Sun J and Stirner T 2003 *Phys. Rev.* E **67** 051107
[131] Zangi R and Rice S A 1998 *Phys. Rev.* E **58** 7529
[132] Loudet J, Yodh A G and Pouligny B 2006 *Phys. Rev. Lett.* **97** 018304
[133] Basavaraj M G, Fuller G G, Fransaer J and Vermant J 2006 *Langmuir* **22** 6605
[134] Bates M A and Frenkel D 2000 *J. Chem. Phys.* **112** 10034
[135] Meldrum F C, Kotov N A and Fendler J H 1994 *J. Phys. Chem.* **98** 4506
[136] Lefebure S, Menager C, Cabuil V, Assenheimer M, Gallet F and Flament C 1998 *J. Phys. Chem.* B **102** 2733
[137] Leunissen M E, van Blaaderen A, Hollingsworth A D, Sullivan M T and Chaikin P M 2007 *Proc. Natl Acad. Sci.* **104** 2585
[138] Hoffmann N, Ebert F, Likos C N, Löwen H and Maret G 2006 *Phys. Rev. Lett.* **97** 078301
[139] Froltsov V A, Blaak R, Likos C N and Löwen H 2003 *Phys. Rev.* E **68** 061406
[140] Stillinger F H 1961 *J. Chem. Phys.* **35** 1584
[141] Hurd A J 1985 *J. Phys. A: Math. Gen.* **18** L1055
[142] Faraudo J and Bresme F 2004 *Phys. Rev. Lett.* **92** 236102
Faraudo J and Bresme F 2005 *Phys. Rev. Lett.* **94** 077802
[143] Williams D F and Berg J C 1992 *J. Colloid Interface Sci.* **152** 218
[144] Hamaker H C 1937 *Physica* **4** 1058
[145] Derjaguin B 1934 *Kolloid Z.* **69** 155
[146] Korgel B A and Fitzmaurice D 1999 *Phys. Rev.* B **59** 14191
[147] Dominguez A, Oettel M and Dietrich S 2005 *J. Phys.: Condens. Matter* **17** S3387
[148] Zeng C, Bissig H and Dinsmore A D 2006 *Solid State Commun.* **139** 547
[149] Würger A 2006 *Europhys. Lett.* **75** 978
[150] Dominguez A, Oettel M and Dietrich S 2007 *Europhys. Lett.* **77** 68002
[151] Oettel M, Dominguez A and Dietrich S 2005 *J. Phys.: Condens. Matter* **17** L337
[152] Würger A and Foret L 2005 *J. Phys. Chem.* B **109** 16435
[153] van Nierop E A, Stijnman M A and Hilgenfeldt S 2005 *Europhys. Lett.* **72** 671
[154] Buff F P, Lovett R A and Stillinger F H 1965 *Phys. Rev. Lett.* **15** 621
[155] Fradin C, Braslau A, Luzet D, Smilgies D, Alba M, Boudet N, Mecke K and Daillant J 2000 *Nature* **403** 871
[156] Seydel T, Madsen A, Tolan M, Grübel G and Press W 2001 *Phys. Rev.* B **63** 073409
[157] Aarts D G A L, Schmidt M and Lekkerkerker H N W 2004 *Science* **304** 847
[158] Casimir H B G 1948 *Proc. K. Ned. Akad. Wet.* **51** 793
[159] Golestanian R 2000 *Phys. Rev.* E **62** 5242
[160] Golestanian R, Goulian M and Kardar M 1996 *Phys. Rev.* E **54** 6725
[161] Hansen J P and McDonald I R 2006 *Theory of Simple Liquids* 3rd edn (London: Academic)
[162] Bresme F, Oettel M and Lehle H 2007 unpublished